# Particles at fluid-fluid interfaces: A new Navier-Stokes-Cahn-Hilliard surface-phase-field-crystal model

Sebastian Aland,[1,*] John Lowengrub,[2,†] and Axel Voigt[1,‡]
[1]*Institut für wissenschaftliches Rechnen, TU Dresden, Dresden, Germany*
[2]*Mathematics Department, University of California, Irvine, California, USA*
(Received 14 May 2012; published 25 October 2012)

Colloid particles that are partially wetted by two immiscible fluids can become confined to fluid-fluid interfaces. At sufficiently high volume fractions, the colloids may jam and the interface may crystallize. The fluids together with the interfacial colloids form an emulsion with interesting material properties and offer an important route to new soft materials. A promising approach to simulate these emulsions was presented in Aland *et al.* [Phys. Fluids **23**, 062103 (2011)], where a Navier-Stokes-Cahn-Hilliard model for the macroscopic two-phase fluid system was combined with a surface phase-field-crystal model for the microscopic colloidal particles along the interface. Unfortunately this model leads to spurious velocities which require very fine spatial and temporal resolutions to accurately and stably simulate. In this paper we develop an improved Navier-Stokes-Cahn-Hilliard-surface phase-field-crystal model based on the principles of mass conservation and thermodynamic consistency. To validate our approach, we derive a sharp interface model and show agreement with the improved diffuse interface model. Using simple flow configurations, we show that the new model has much better properties and does not lead to spurious velocities. Finally, we demonstrate the solid-like behavior of the crystallized interface by simulating the fall of a solid ball through a colloid-laden multiphase fluid.

DOI: 10.1103/PhysRevE.86.046321 PACS number(s): 47.10.A−, 47.11.Fg, 47.57.−s

## I. INTRODUCTION

Bicontinuous gels are widely used in many fields of daily life such as the food, cosmetic, and pharmaceutical industries. They are used to deliver drug compounds, fragrances, or flavors. Stability of the bicontinuous gel is essential for such purposes. A bicontinuous gel consists of interpenetrating, continuous domains of two immiscible fluids. Due to interfacial tension at the fluid-fluid interfaces such structures are not stable and are subject to coarsening. In order to maintain a bicontinuous state and prevent the structure from coarsening, amphiphilic molecules such as surfactants and polymers can be used to reduce the interfacial tension significantly thereby slowing the coarsening process. However, bicontinuous gels can also be stabilized using colloidal particles, in analogy with stabilized (Pickering) emulsions [1–5]. In so-called "bijels" (bicontinuous interfacially jammed emulsions gels) the structure is stabilized by a jammed layer of colloidal particles at the interface. Such gels were initially proposed on the basis of computer simulations [6] and later were experimentally confirmed [7]. For a review on both theoretical and experimental approaches we refer the reader to [8]. The basic ideas behind the formation of bijels are (1) generation of a bicontinuous structure by spinodal decomposition or intense mixing, (2) adsorption of colloidal particles at interfaces, and (3) jamming of interface colloids either by a reduction in surface area of interfaces or by sufficiently high volume fractions of interfacial colloids. If the layer of colloidal particles at the interface truly solidifies a three-dimensional solid gel with finite elastic modulus and yield stress is formed. Such an amorphous structure with fluid bicontinuity and yield stress forms a novel class of materials. However, the stability of these materials is still under debate. It is not known whether the system is stable for long times and what are the mechanisms that ensure stability. For example, it remains an open question whether attraction between the colloids is essential for stability, or if repulsive particle interactions can lead to stable configurations as well.

Using computer simulations to understand the dynamic properties of bijels is a promising approach. However, there are various shortcomings of traditional approaches due to the very different spatiotemporal scales involved. On the one hand, fluid dynamics have to be considered in mesoscopic time and spatial scales resolving the bicontinuous domain structures. On the other hand, the motion of colloidal particles and particle-particle interactions have to be considered. Further, the particle size is in the nano- or micrometer range. Lattice Boltzmann methods have been applied for the description of the fluid. These methods can be combined with molecular dynamic algorithms to simulate particles in a flow; see e.g., Refs. [6,9–13]. However, this approach can only partly account for the different temporal scales. The Lattice Boltzmann approach is well suited to account for the small time scales of the particle-particle interactions, but it reaches its limits when long-term evolutions are considered, e.g., the essential questions of long-time stability of bijels.

Alternatively, the Navier-Stokes equations can be used to describe the fluids on the large time scales of interest for investigations on stability. However, an incorporation of colloidal particles into such an approach leads to limitations on the size of the system. A first attempt in this direction is given in Ref. [14]. The approach involves a diffuse-interface

*sebastian.aland@tu-dresden.de
†Corresponding author: Also at Materials Science and Engineering Department, University of California, Irvine; lowengrb@math.uci.edu.
‡Also at Center for Advanced Modeling and Simulation, TU Dresden, Dresden, Germany; axel.voigt@tu-dresden.de

 

description of the fluid phases, in addition to a collection of solid particles. However, this approach requires the resolution of the short particle-particle interaction time scales.

In Ref. [15] a different approach is considered, which models the colloidal particles using a classical dynamic density functional theory (DDFT) approach. This enables the simulation of particle-particle interactions on diffusive time scales by averaging out the vibrational modes. Combined with a two-phase Navier-Stokes equation this gives a promising way to simulate bijels over a long time frame, while resolving the particle interactions appropriately by accounting for particle-particle correlations on the meso- and macroscales. The approach combines a classical Navier-Stokes-Cahn-Hilliard equation to model the two-phase flow system, with a surface phase field crystal model for the colloidal particle interactions. The phase field crystal model, first introduced to describe elasticity in crystalline materials [16], is a local approximation of a classical dynamic density functional theory [17]. The approach is used for crystallization of surfaces in Ref. [18]. A derivation of the model from classical dynamic density functional theory in this context can be found in Ref. [19].

The Navier-Stokes-Cahn-Hilliard surface-phase-field-crystal (NSCHSPFC) model developed in Ref. [15] introduced a new elastic force resulting from the colloidal particle interactions. This force acts in addition to the interfacial tension on the fluid-fluid interface. The approach thus differs from the modeling in Ref. [13], in which the colloidal particles affect only the interfacial tension. The NSCHSPFC model is thermodynamically consistent and enables studies to be performed of the effect of attractive or repulsive particle interactions on the stability of fluid domains. Combined with classical models for surfactants, which influence only the interfacial tension (see, e.g., Ref. [20]), the NSCHSPFC approach can also be used to model more recent experimental investigations on the influence of surfactants on particle-stabilized gels [21].

However, numerical investigations of the NSCHSPFC model presented in Ref. [15] show severe limitations of the approach due to the development of spurious velocities close to the interface. This requires small time steps and a high spatial resolution to accurately and stably simulate, which makes three-dimensional simulations very expensive. The aim of the paper is to improve the NSCHSPFC model to suppress these spurious velocities by deriving a new form of the elastic force. After a brief review of the model introduced in Ref. [15] we consider various ways to derive the new elastic force. The first attempt considers an averaging of the elastic force over a vanishingly small control volume at the interface. The second attempt derives a set of equations within a diffuse interface approach by using an appropriate approximation of a surface delta function. The elastic force thus obtained coincides with the elastic force found by averaging over the control volume. To confirm the results further a sharp interface model is also derived, and it is demonstrated that the diffuse interface equations approximate the sharp interface system. Numerical investigations of the diffuse interface model show that spurious velocities are suppressed. The new approach enables three-dimensional simulations to be performed, which are used to demonstrate that the colloidal particle interactions can stabilize bicontinuous gels. We also demonstrate an advantage of the diffuse interface approach, namely, the ease in which additional physical processes may be incorporated, and we simulate a rigid body falling within a particle-stabilized gel.

The outline of the paper is as follows. In Sec. II the NSCHSPFC model from Ref. [15] is briefly reviewed. In Sec. III a regularized elastic force is derived by averaging the elastic force from Ref. [15] over a vanishingly small control volume. In Sec. IV a new, variational NSCHSPFC model is derived using a new approximation of the surface delta function. In Sec. V a new sharp interface model is derived, and the new variational model is shown to be a diffuse interface approximation of the sharp interface system. In Sec. VI the methods used to solve the NSCHSPFC system are briefly discussed. In Sec. VII numerical results are presented, and conclusions are drawn in Sec. VIII.

## II. THE NSCHSPFC MODEL: A BRIEF REVIEW

In this section, we briefly review the NSCHSPFC model which was derived in Ref. [15] using an energy variation approach. We denote all variables in nondimensional form. Time and space are nondimensionalized by $t' = t/\tau_\sigma$ and $x' = x/L$ where $\tau_\sigma = \sqrt{\rho_{\text{fluid}} L^3/\sigma}$ is the characteristic time associated with surface tension relaxation, with $\sigma$ being the surface tension and $\rho_{\text{fluid}}$ the density of the fluid, which is assumed to be constant for simplicity. The parameter $L$ is a measure of the characteristic size of the fluid domain (e.g., drop radius). Hereafter, we drop the prime notation.

The foundation of the NSCHSPFC model is a representation of the two immiscible fluids by a phase field variable $\psi$ such that $\psi = 0$ and 1 denote the two fluid phases and $\psi = 0.5$ denotes the interface location: $\Gamma(t) = \{\mathbf{x} \in \Omega : \psi(\mathbf{x},t) = 0.5\}$, with $\Omega \subset I\!R^{2,3}$. For example, one may take

$$\psi(\mathbf{x},t) = \frac{1}{2}\left\{1 - \tanh\left[\frac{d(\mathbf{x},t)}{\sqrt{2}\epsilon}\right]\right\}, \tag{1}$$

where $\epsilon$ determines the interface thickness and $d(\mathbf{x},t)$ denotes the signed distance function from the fluid-fluid interface to $\mathbf{x}$ at time $t$. For this choice of $\psi$, a calculation shows that the function

$$B(\psi) = \psi^2(1-\psi)^2, \tag{2}$$

when scaled by $6\sqrt{2}/\epsilon$, approximates the surface delta function $\delta_\Gamma$:

$$\frac{6\sqrt{2}}{\epsilon} B(\psi) \approx \delta_\Gamma. \tag{3}$$

Rather than defining $\psi$ by Eq. (1), it can be determined by solving an advective Cahn-Hilliard equation whose solution near $\Gamma$ approximates Eq. (1) for small $\epsilon$.

Furthermore, we define $\rho_c$ to be the nondimensional colloid number density. Here we take $\rho_c = \rho + \tilde{\rho}$, where $\tilde{\rho}$ is a constant nondimensional equilibrium colloid density and $\rho$ is the deviation from equilibrium. Then, the elastic energy of the colloidal system on the surface can be approximated by the so-called Surface Phase Field Crystal (SPFC) energy [15]:

$$E_{\text{spfc}} = \frac{\text{El}^{-1}}{\epsilon} \int_\Omega B(\psi) f(\rho, \nabla\rho, \nu)\, dx, \tag{4}$$

with the SPFC energy density $f(\rho,\nabla\rho,\nu)$ given by

$$f(\rho,\nabla\rho,\nu) = \frac{1}{4}\rho^4 + \frac{1+r}{2}\rho^2 - \delta^2|\nabla\rho|^2 + \frac{\delta^4}{2}\nu^2, \quad (5)$$

$$\nu = \frac{1}{B(\psi)}\nabla\cdot[B(\psi)\nabla\rho]. \quad (6)$$

El is an elasticity number which measures the relative strength of the elastic energy (to the surface energy), $r$ is a nondimensional parameter that arises from the structure factor for the colloidal system, and $\delta = L_c/L$ is the ratio of the characteristic length scales of the colloid and fluid systems.

We now suppose that the total energy of the system consists of the SPFC energy, the surface energy $E_\sigma$, and the kinetic energy $E_{\rm kin}$:

$$E = E_{\rm spfc} + E_\sigma + E_{\rm kin}, \quad (7)$$

where in nondimensional form the surface energy is approximated by the Cahn-Hilliard energy

$$E_\sigma = \frac{1}{\epsilon}\int_\Omega B(\psi) + \frac{\epsilon^2}{2}|\nabla\psi|^2\,dx \quad (8)$$

and the kinetic energy is

$$E_{\rm kin} = \frac{1}{2}\int_\Omega |\mathbf{u}|^2\,dx, \quad (9)$$

with velocity $\mathbf{u}$, where we have assumed that the fluid components are density-matched and the velocity is nondimensionalized by $U = L/\tau_\sigma$ (see Ref. [15]). Using an energy variation argument the following governing equations for the two-phase system with colloidal particles can be derived [15]. We write the equations as a system of second order partial differential equations. The advective Cahn-Hilliard equation governs the motion of the two-phase interface:

$$\partial_t\psi + \mathbf{u}\cdot\nabla\psi = {\rm Pe}_\psi^{-1}\epsilon\nabla\cdot[B(\psi)\nabla\mu], \quad (10)$$

$$\mu = \epsilon^{-1}B'(\psi) - \epsilon\Delta\psi. \quad (11)$$

The SPFC equation on the diffuse interface defined by $\psi$ governs the evolution of the surface colloids [15]:

$$\partial_t[B(\psi)(\rho+\tilde\rho)] + \nabla\cdot[B(\psi)\mathbf{u}(\rho+\tilde\rho)] = {\rm Pe}_\rho^{-1}\nabla\cdot[B(\psi)\nabla\omega], \quad (12)$$

$$B(\psi)\omega = B(\psi)\rho(\rho^2+1+r) + 2\delta^2 B(\psi)\nu + \delta^4\nabla\cdot[B(\psi)\nabla\nu], \quad (13)$$

$$B(\psi)\nu = \nabla\cdot[B(\psi)\nabla\rho], \quad (14)$$

where $\tilde\rho$ is defined below. Finally, the Navier-Stokes equations, with surface tension and elastic forces, governs the motion of the fluids:

$$\partial_t\mathbf{u} + (\mathbf{u}\cdot\nabla)\mathbf{u} = -\nabla\bar p + \frac{1}{\rm Re}\Delta\mathbf{u} + \mu\nabla\psi + \frac{{\rm El}^{-1}}{\epsilon}B(\psi)\omega\nabla\rho + \mathbf{F}_{\rm el}, \quad (15)$$

$$\nabla\cdot\mathbf{u} = 0, \quad (16)$$

with a rescaled pressure $\bar p$ and the elastic force

$$\mathbf{F}_{\rm el} = \frac{{\rm El}^{-1}}{\epsilon}\nabla B(\psi)(f - \delta^4\nabla\nu\cdot\nabla\rho - \delta^4\nu^2). \quad (17)$$

Here ${\rm Pe}_\psi$ and ${\rm Pe}_\rho$ are Peclet numbers and Re is the Reynolds number. Finally the NSCHSPFC system is equipped with the initial conditions

$$\mathbf{u}(t=0,\mathbf{x}) = \mathbf{u}_0(\mathbf{x}), \quad \psi(t=0,\mathbf{x}) = \psi_0(\mathbf{x}),$$
$$\rho(t=0,\mathbf{x}) = \rho_0(\mathbf{x}), \quad \text{in } \Omega$$

and either natural boundary conditions

$$\frac{\partial\psi}{\partial\mathbf{n}} = \frac{\partial\rho}{\partial\mathbf{n}} = \frac{\partial\mu}{\partial\mathbf{n}} = \frac{\partial\nu}{\partial\mathbf{n}} = \frac{\partial\omega}{\partial\mathbf{n}} = 0, \qquad \mathbf{u} = \mathbf{u}_\infty \quad \text{on } \partial\Omega,$$

where $\mathbf{n}$ denotes the outward normal vector or periodic boundary conditions.

Note that the above sixth order, nonlinear, and nonlocal equations are a simplification of the governing equations presented in Ref. [15], which included extra terms describing attachment and detachment of colloids from the bulk to the surface. Also note that the evolution equations for the colloid number density (12)–(14) corresponds to the form from the original paper with the substitution $\rho \to \rho + \tilde\rho$, where $\tilde\rho$ is a nondimensional physical constant given by $\tilde\rho = \sqrt{g/(\beta q_0^4)}$ with system specific parameters $\beta$, $g$, and $q_0$ (see Ref. [22]). This leads to the physically correct conservation of $\rho + \tilde\rho$ on the interface.

## III. A REGULARIZED ELASTIC FORCE

It was demonstrated in Ref. [15] that the NSCHSPFC model presented in the previous section is capable of describing, at least phenomenologically, two-phase systems where colloids are present at the interface. The crucial part is the force $\mathbf{F}_{\rm el}$, which we refer to as elastic force, since it comes from the colloid interactions introduced by the SPFC energy. It has been shown that this force induces strong local straining flows around the interface, which require small time steps and a fine grid to be resolved [15].

We will now present a way to regularize $\mathbf{F}_{\rm el}$ which can eliminate the spurious flows. The idea is to average $\mathbf{F}_{\rm el}$ over a control volume located at the interface and then take the limit as the control volume becomes infinitesimally small. To do this, we will restrict ourselves to two dimensions and consider a single point $x_0$ on the interface (see Fig. 1). We define a control volume with tangential thickness $\Delta s$ and normal thickness $\Delta z$, which we assume large enough to capture all of the nonzero part of $\mathbf{F}_{\rm el}$ in a vicinity of $x_0$, e.g., $\epsilon \ll \Delta z$. If we now calculate the integral of $\mathbf{F}_{\rm el}$ over V and let $\Delta s$ tend to zero, we will get the effective force acting on the interface at $x_0$.

A coordinate point $x$ in $V$ can be expressed using the arc length $s$ and the normal distance $z$ by

$$x(s,z) = \left(\frac{1}{\kappa} + z\right)(\cos(\alpha+\kappa s), \sin(\alpha+\kappa s)), \quad (18)$$

where $\kappa$ is the curvature of the interface at the point $x(s,0)$. The Jacobian matrix of this coordinate transformation

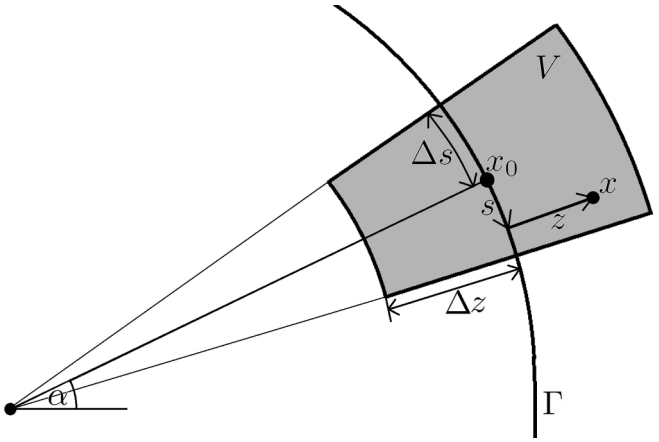


FIG. 1. The control volume $V$ defined around an arbitrary interface point $x_0$.

reads

$$J = \begin{pmatrix} \cos(\alpha+\kappa s) & -(1+\kappa z)\sin(\alpha+\kappa s) \\ \sin(\alpha+\kappa s) & (1+\kappa z)\cos(\alpha+\kappa s) \end{pmatrix}. \tag{19}$$

Now, we consider the integral of $\mathbf{F}_{el}$ over the volume $V$:

$$\int_V \mathbf{F}_{\text{el}}\,dx = \int_{-\Delta s}^{\Delta s}\int_{-\Delta z}^{\Delta z} \mathbf{F}_{\text{el}}|J|\,dz\,ds \tag{20}$$

$$= \int_{-\Delta s}^{\Delta s}\int_{-\Delta z}^{\Delta z} \mathbf{F}_{\text{el}}(1+\kappa z)\,dz\,ds \tag{21}$$

$$= \frac{\text{El}^{-1}}{\epsilon}\int_{-\Delta s}^{\Delta s}\int_{-\Delta z}^{\Delta z} \nabla B(\psi)\left(\frac{1}{4}\rho^4 + \frac{1+r}{2}\rho^2 - \delta^2|\nabla\rho|^2 - \frac{\delta^4}{2}\nu^2 - \delta^4\nabla\nu\cdot\nabla\rho\right)(1+\kappa z)\,dz\,ds. \tag{22}$$

Since $\rho$ and $\nu$ are constant in the normal direction to first order, it holds

$$\rho(x(s,z)) \approx \rho(x(s,0)), \quad \nu(x(s,z)) \approx \nu(x(s,0)) \tag{23}$$

and consequently

$$\begin{aligned} \nabla\rho(x(s,z)) &\approx \nabla\rho(x(s,0))\frac{1}{1+\kappa z}, \\ \nabla\nu(x(s,z)) &\approx \nabla\nu)x(s,0))\frac{1}{1+\kappa z}. \end{aligned} \tag{24}$$

Using this in Eq. (22) we get

$$\begin{aligned} \int_V \mathbf{F}_{\text{el}}\,dx \approx{}& \frac{\text{El}^{-1}}{\epsilon}\int_{-\Delta s}^{\Delta s}\left(\frac{1}{4}\rho^4 + \frac{1+r}{2}\rho^2 - \frac{\delta^4}{2}\nu^2\right)(x(s,0)) \\ &\cdot \int_{-\Delta z}^{\Delta z} \nabla B(\psi)(1+\kappa z)\,dz\,ds \\ &- \frac{\text{El}^{-1}}{\epsilon}\int_{-\Delta s}^{\Delta s}(\delta^2|\nabla\rho|^2 + \delta^4\nabla\nu\cdot\nabla\rho)(x(s,0)) \\ &\cdot \int_{-\Delta z}^{\Delta z} \nabla B(\psi)\frac{1}{1+\kappa z}\,dz\,ds. \end{aligned} \tag{25}$$

Using that $B = \psi^2(1-\psi)^2$ and Eq. (1), the integrals over $z$ can be approximated analytically. As $\epsilon \to 0$ we obtain

$$\int_{-\Delta z}^{\Delta z} \nabla B(\psi)(1+\kappa z)\,dz \to -\frac{1}{6\sqrt{2}}\epsilon\mathbf{n}\kappa, \tag{26}$$

$$\int_{-\Delta z}^{\Delta z} \nabla B(\psi)\frac{1}{1+\kappa z}\,dz \to +\frac{1}{6\sqrt{2}}\epsilon\mathbf{n}\kappa. \tag{27}$$

Hence, we get

$$\int_V \mathbf{F}_{\text{el}}\,dx \approx -\frac{\text{El}^{-1}}{6\sqrt{2}}\int_{-\Delta s}^{\Delta s}\kappa\mathbf{n}g(x(s,0))\,ds, \tag{28}$$

where

$$g := \frac{1}{4}\rho^4 + \frac{1+r}{2}\rho^2 - \frac{\delta^4}{2}\nu^2 + \delta^2|\nabla\rho|^2 + \delta^4\nabla\nu\cdot\nabla\rho. \tag{29}$$

Hence, we have

$$\int_V \mathbf{F}_{\text{el}}\,dx = \int_V -\frac{\text{El}^{-1}}{6\sqrt{2}}\delta_\Gamma\kappa\mathbf{n}g\,ds, \tag{30}$$

with a Dirac interface delta function $\delta_\Gamma$. Now, letting the control volume $V$ become infinitesimal small by taking $\Delta s \to 0$ leads to the point force

$$\mathbf{F}_{\text{new}} := -\frac{\text{El}^{-1}}{6\sqrt{2}}\delta_\Gamma\kappa\mathbf{n}g \tag{31}$$

at $x_0$. Since the above calculations hold for arbitrary $x_0$, this point force is valid in every interface point. Note that $\mathbf{F}_{\text{new}}$ can be seen as the sharp interface version of $\mathbf{F}_{\text{el}}$, which we confirm in Sec. V. Now, we can use the Cahn Hilliard chemical potential to approximate the curvature and hence get a diffuse interface version of $\mathbf{F}_{\text{new}}$. To be more precise, for $\epsilon \to 0$ we have

$$\mu\nabla\psi \to -\frac{1}{3\sqrt{2}}\kappa\delta_\Gamma\mathbf{n}, \tag{32}$$

which leads to the approximation

$$\mathbf{F}_{\text{new}} \approx \frac{\text{El}^{-1}}{2}g\mu\nabla\psi. \tag{33}$$

Now, the new governing equations are (10)–(16) with $\mathbf{F}_{\text{el}}$ in Eq. (15) replaced by $\mathbf{F}_{\text{new}}$:

$$\partial_t\mathbf{u} + (\mathbf{u}\cdot\nabla)\mathbf{u} = -\nabla\bar{p} + \frac{1}{\text{Re}}\Delta\mathbf{u} + \mu\nabla\psi + \frac{\text{El}^{-1}}{\epsilon}B(\psi)\omega\nabla\rho + \mathbf{F}_{\text{new}}. \tag{34}$$

Note that the new system converges to the old system as $\epsilon \to 0$, since $\mathbf{F}_{\text{el}} \to \mathbf{F}_{\text{new}}$. We confirm in Sec. VII A, that the new elastic force eliminates spurious velocities and leads to improved properties of the system.

## IV. A VARIATIONAL DIFFUSE INTERFACE MODEL

In this section we will present a variational approach to derive a diffuse interface system containing the new elastic force. To do so, we introduce a new approximation to the surface delta function,

$$e = \frac{\epsilon^2}{4}|\nabla\psi|^2 + \frac{1}{2}B(\psi), \tag{35}$$

which has the same scaling to the surface delta function as $B$. This form of an approximation to the surface delta function has already been used in Refs. [23,24]. Now, we use $e$ instead of $B$ to restrict the PFC energy to the interface:

$$\tilde{E}_{\text{spfc}} = \frac{\text{El}^{-1}}{\epsilon}\int_\Omega e\tilde{f}\,dx, \quad \text{with} \tag{36}$$

$$\tilde{f} = \frac{1}{4}\rho^4 + \frac{1+r}{2}\rho^2 - \delta^2|\nabla\rho|^2 + \frac{\delta^4}{2}\tilde{\nu}^2, \tag{37}$$

$$\tilde{\nu} = \frac{1}{e}\nabla\cdot(e\nabla\rho). \tag{38}$$

Note that we will use the tilde notation to distinguish variables that differ from the original model. The total energy to be considered is now

$$\tilde{E} = \tilde{E}_{\text{spfc}} + E_\sigma + E_{\text{kin}}. \tag{39}$$

### A. Energy variation

We now derive the equations for the two-phase system with colloidal particles starting with an energy variation argument. To do so, we suppose the fluid motion is governed by the Navier-Stokes equations, which are given by

$$\dot{\mathbf{u}} = -\mathbf{u}\cdot\nabla\mathbf{u} - \nabla p + \frac{1}{\text{Re}}\Delta\mathbf{u} + \tilde{\mathbf{F}}, \nabla\cdot\mathbf{u} = 0, \tag{40}$$

where $p$ is the pressure and the force $\tilde{\mathbf{F}}$ is as yet unspecified. Note that if Re is small, the Stokes equations could be used instead of the Navier-Stokes equations, and the analysis below remains valid. It is often useful to represent forces in the Navier-Stokes equation as the divergence of a stress tensor. Hence, our goal will be to derive a singular stress tensor, whose divergence will be $\tilde{\mathbf{F}}$. Furthermore, the functions $\psi$ and $\rho$ are assumed to satisfy the conservation equations

$$\dot{\psi} = -\mathbf{u}\cdot\nabla\psi - \nabla\cdot\tilde{\mathbf{J}}_\psi, \tag{41}$$

$$\frac{\partial}{\partial t}[e(\rho+\tilde{\rho})] = -\nabla\cdot[e\mathbf{u}(\rho+\tilde{\rho})] - \nabla\cdot\tilde{\mathbf{J}}_\rho, \tag{42}$$

where the fluxes $\tilde{\mathbf{J}}_\rho$ and $\tilde{\mathbf{J}}_\psi$ have also not yet been specified. Note that Eq. (42) is the basic diffuse interface form of the surface mass conservation equation [20,25,26]. Using the incompressibility of the fluid and Eqs. (41) and (42) can be rewritten as

$$e(\dot{\rho} + \mathbf{u}\cdot\nabla\rho) = -(\rho+\tilde{\rho})(\dot{e} + \mathbf{u}\cdot\nabla e) - \nabla\cdot\tilde{\mathbf{J}}_\rho. \tag{43}$$

We next take the time derivative of the energy $\tilde{E}$ and insert the previously defined evolution equations for $\rho$, $\psi$, and $\mathbf{u}$. Requiring that $\dot{\tilde{E}} \leqslant 0$, where the overdot denotes the time derivative, enables us to pose constitutive relations for the singular stress tensor and fluxes. First, we compute

$$\dot{E}_{\text{kin}} = \int_\Omega \mathbf{u}\dot{\mathbf{u}}\,dx. \tag{44}$$

Inserting Eq. (40) into Eq. (44) and integrating by parts gives

$$\dot{E}_{\text{kin}} = \int_\Omega -\frac{1}{\text{Re}}\nabla\mathbf{u} : \nabla\mathbf{u} + \mathbf{u}\cdot\tilde{\mathbf{F}}\,dx, \tag{45}$$

where $\nabla\mathbf{u} : \nabla\mathbf{u} = (\frac{\partial \mathbf{u}_i}{\partial x_j})\frac{\partial \mathbf{u}_i}{\partial x_j}$. Next, we consider the surface energy $E_\sigma$ and get

$$\dot{E}_\sigma = \int_\Omega \frac{1}{\epsilon}B'(\psi)\dot{\psi} + \epsilon\nabla\psi\cdot\nabla\dot{\psi}\,dx. \tag{46}$$

Inserting (41) yields

$$\begin{aligned}\dot{E}_\sigma &= \int_\Omega -\frac{1}{\epsilon}B'(\psi)\nabla\psi\cdot\mathbf{u} - \epsilon\nabla\psi\cdot\nabla\nabla\psi\cdot\mathbf{u} - \epsilon\nabla\psi\cdot\nabla\mathbf{u}\\ &\quad\cdot\nabla\psi - \frac{1}{\epsilon}B'(\psi)\nabla\cdot\tilde{\mathbf{J}}_\psi - \epsilon\nabla\psi\cdot\nabla\nabla\cdot\tilde{\mathbf{J}}_\psi\,dx \qquad (47)\\ &= \int_\Omega -\mathbf{u}\cdot\nabla\left[\frac{1}{\epsilon}B(\psi) + \frac{\epsilon}{2}|\nabla\psi|^2\right] - \epsilon\nabla\psi\otimes\nabla\psi : \nabla\mathbf{u}\\ &\quad - \frac{1}{\epsilon}B'(\psi)\nabla\cdot\tilde{\mathbf{J}}_\psi - \epsilon\nabla\psi\cdot\nabla\nabla\cdot\tilde{\mathbf{J}}_\psi\,dx. \qquad (48)\end{aligned}$$

Integrating by parts and dropping all boundary terms gives

$$\begin{aligned}\dot{E}_\sigma &= \int_\Omega \mathbf{u}\cdot\nabla\cdot(\epsilon\nabla\psi\otimes\nabla\psi)\\ &\quad - \left[\frac{1}{\epsilon}B'(\psi) + \epsilon\nabla\psi\cdot\nabla\right]\nabla\cdot\tilde{\mathbf{J}}_\psi\,dx. \qquad (49)\end{aligned}$$

Next, we can compute

$$\begin{aligned}\dot{\tilde{E}}_{\text{spfc}} &= \frac{\text{El}^{-1}}{\epsilon}\int_\Omega \dot{e}\tilde{f} + e\dot{\tilde{f}}\,dx \qquad (50)\\ &= \frac{\text{El}^{-1}}{\epsilon}\int_\Omega \tilde{f}(\dot{e} + \mathbf{u}\cdot\nabla e) + e(\dot{\tilde{f}} + \mathbf{u}\cdot\nabla\tilde{f})\\ &\quad - \mathbf{u}\cdot\nabla(e\tilde{f})\,dx \qquad (51)\\ &= \frac{\text{El}^{-1}}{\epsilon}\int_\Omega \tilde{f}(\dot{e} + \mathbf{u}\cdot\nabla e) + e(\dot{\tilde{f}} + \mathbf{u}\cdot\nabla\tilde{f})\,dx. \qquad (52)\end{aligned}$$

Now, we will evaluate $\int_\Omega e(\dot{\tilde{f}} + \mathbf{u}\cdot\nabla\tilde{f})\,dx$. To make the calculations clearer, we split $\tilde{f}$ into its zero order part $\tilde{f}_0 = \frac{1}{4}\rho^4 + \frac{1+r}{2}\rho^2$, its first order part $\tilde{f}_1 = -\delta^2|\nabla\rho|^2$, and its second order part $\tilde{f}_2 = \frac{\delta^4}{2}\tilde{\nu}^2$. Accordingly, we obtain

$$\begin{aligned}&\int_\Omega e(\dot{\tilde{f}}_0 + \mathbf{u}\cdot\nabla\tilde{f}_0)\,dx\\ &= \int_\Omega e(\dot{\rho} + \mathbf{u}\cdot\nabla\rho)(\rho^3 + (1+r)\rho)\,dx, \qquad (53)\\ &\int_\Omega e(\dot{\tilde{f}}_1 + \mathbf{u}\cdot\nabla\tilde{f}_1)\,dx\\ &= \int_\Omega -2e\delta^2\nabla\rho\nabla\dot{\rho} - 2e\delta^2\nabla\nabla\rho : (\nabla\rho\otimes\mathbf{u})\,dx \qquad (54)\\ &= \int_\Omega 2e\delta^2\tilde{\nu}(\dot{\rho} + \mathbf{u}\cdot\nabla\rho) + 2e\delta^2\nabla\mathbf{u} : (\nabla\rho\otimes\nabla\rho)\,dx \qquad (55)\\ &= \int_\Omega 2e\delta^2\tilde{\nu}(\dot{\rho} + \mathbf{u}\cdot\nabla\rho) - \mathbf{u}\cdot\nabla\cdot(2e\delta^2\nabla\rho\otimes\nabla\rho)\,dx,\end{aligned}$$

(56)

and

$$\int_\Omega e(\dot{\tilde{f}}_2 + \mathbf{u}\cdot\nabla\tilde{f}_2)\,dx = \delta^4\int_\Omega -\tilde{\nu}^2(\dot{e}+\mathbf{u}\cdot\nabla e) + \tilde{\nu}\nabla\cdot(\dot{e}\nabla\rho) + \tilde{\nu}\mathbf{u}\cdot\nabla\cdot(\nabla\rho\otimes\nabla e) + \tilde{\nu}\nabla\cdot(e\nabla\dot{\rho}) + \tilde{\nu}\mathbf{u}\cdot\nabla\cdot(e\nabla\nabla\rho)\,dx \tag{57}$$

$$= \delta^4\int_\Omega -\tilde{\nu}^2(\dot{e}+\mathbf{u}\cdot\nabla e) - (\nabla\tilde{\nu}\cdot\nabla\rho)\dot{e} - e\nabla\tilde{\nu}\cdot\nabla\dot{\rho} + \tilde{\nu}\mathbf{u}\cdot\nabla\cdot[\nabla(e\nabla\rho)^T]\,dx \tag{58}$$

$$= \delta^4\int_\Omega -\tilde{\nu}^2(\dot{e}+\mathbf{u}\cdot\nabla e) - (\nabla\tilde{\nu}\cdot\nabla\rho)\dot{e} + \nabla\cdot(e\nabla\tilde{\nu})\dot{\rho} + \tilde{\nu}\mathbf{u}\cdot\nabla\cdot[\nabla(e\nabla\rho)]^T\,dx. \tag{59}$$

Now, we can use that

$$\tilde{\nu}\mathbf{u}\cdot\nabla\cdot(\nabla(e\nabla\rho))^T = \mathbf{u}\cdot\nabla\cdot[\tilde{\nu}\nabla(e\nabla\rho)]^T - \mathbf{u}\cdot\nabla(e\nabla\rho)\cdot\nabla\tilde{\nu} \tag{60}$$

$$= \mathbf{u}\cdot\nabla\cdot[\tilde{\nu}\nabla(e\nabla\rho)]^T - \mathbf{u}\cdot\nabla e\nabla\tilde{\nu}\cdot\nabla\rho - e\mathbf{u}\cdot\nabla\nabla\rho\cdot\nabla\tilde{\nu} \tag{61}$$

$$= \mathbf{u}\cdot\nabla\cdot[\tilde{\nu}\nabla(e\nabla\rho)]^T - \mathbf{u}\cdot\nabla e\nabla\tilde{\nu}\cdot\nabla\rho - \mathbf{u}\cdot\nabla\cdot(e\nabla\tilde{\nu}\otimes\nabla\rho) + \nabla\cdot(e\nabla\tilde{\nu})\mathbf{u}\cdot\nabla\rho \tag{62}$$

$$= \mathbf{u}\cdot\nabla\cdot[\nabla(\tilde{\nu}e\nabla\rho)]^T - \mathbf{u}\cdot\nabla\cdot(e\nabla\rho\otimes\nabla\tilde{\nu}) - \mathbf{u}\cdot\nabla e\nabla\tilde{\nu}\cdot\nabla\rho - \mathbf{u}\cdot\nabla\cdot(e\nabla\tilde{\nu}\otimes\nabla\rho) + \nabla\cdot(e\nabla\tilde{\nu})\mathbf{u}\cdot\nabla\rho \tag{63}$$

$$= \mathbf{u}\cdot\nabla(\nabla\cdot(\tilde{\nu}e\nabla\rho)) - \mathbf{u}\cdot\nabla\cdot(e\nabla\rho\otimes\nabla\tilde{\nu}) - \mathbf{u}\cdot\nabla e\nabla\tilde{\nu}\cdot\nabla\rho - \mathbf{u}\cdot\nabla\cdot(e\nabla\tilde{\nu}\otimes\nabla\rho) + \nabla\cdot(e\nabla\tilde{\nu})\mathbf{u}\cdot\nabla\rho. \tag{64}$$

Inserting Eq. (64) into Eq. (59) yields

$$\int_\Omega e(\dot{\tilde{f}}_2 + \mathbf{u}\cdot\nabla\tilde{f}_2)\,dx = \delta^4\int_\Omega -(\tilde{\nu}^2 + \nabla\tilde{\nu}\cdot\nabla\rho)(\dot{e}+\mathbf{u}\cdot\nabla e) + \nabla\cdot(e\nabla\tilde{\nu})(\dot{\rho}+\mathbf{u}\cdot\nabla\rho) - \mathbf{u}\cdot\nabla\cdot(e\nabla\tilde{\nu}\otimes\nabla\rho + e\nabla\rho\otimes\nabla\tilde{\nu})\,dx. \tag{65}$$

Now, let us put Eqs. (53), (56), and (65) together to get

$$\int_\Omega e(\dot{\tilde{f}} + \mathbf{u}\cdot\nabla\tilde{f})\,dx = \int_\Omega -\delta^4(\tilde{\nu}^2 + \nabla\tilde{\nu}\cdot\nabla\rho)(\dot{e}+\mathbf{u}\cdot\nabla e) + e(\dot{\rho}+\mathbf{u}\cdot\nabla\rho) \times\left[\rho^3 + (1+r)\rho + 2\delta^2\tilde{\nu} + \frac{\delta^4}{e}\nabla\cdot(e\nabla\tilde{\nu})\right] - \mathbf{u}\cdot\nabla\cdot(2\delta^2 e\nabla\rho\otimes\nabla\rho + \delta^4 e\nabla\tilde{\nu}\otimes\nabla\rho + \delta^4 e\nabla\rho\otimes\nabla\tilde{\nu})\,dx. \tag{66}$$

We can insert Eq. (66) into Eq. (52), which gives

$$\dot{\tilde{E}}_{\text{spfc}} = \int_\Omega \frac{\text{El}^{-1}}{\epsilon}(\tilde{f} - \delta^4\tilde{\nu}^2 - \delta^4\nabla\tilde{\nu}\cdot\nabla\rho)(\dot{e}+\mathbf{u}\cdot\nabla e) + e(\dot{\rho}+\mathbf{u}\cdot\nabla\rho)\frac{\delta\tilde{E}}{\delta\rho} - \frac{\text{El}^{-1}}{\epsilon}\mathbf{u}\cdot\nabla\cdot(2\delta^2 e\nabla\rho\otimes\nabla\rho + \delta^4 e\nabla\tilde{\nu}\otimes\nabla\rho + \delta^4 e\nabla\rho\otimes\nabla\tilde{\nu})\,dx, \tag{67}$$

where we have introduced

$$\frac{\delta\tilde{E}}{\delta\rho} := \frac{\text{El}^{-1}}{\epsilon}\left[\rho^3 + (1+r)\rho + 2\delta^2\tilde{\nu} + \frac{\delta^4}{e}\nabla\cdot(e\nabla\tilde{\nu})\right]. \tag{68}$$

Note that the notation $\frac{\delta\tilde{E}}{\delta\rho}$ makes sense, since the material derivative of $\rho$ is multiplied with this term in the energy time derivative. Now, let us insert the evolution equation for $\rho$ from Eq. (43). We obtain

$$\dot{\tilde{E}}_{\text{spfc}} = \int_\Omega\left[\frac{\text{El}^{-1}}{\epsilon}(\tilde{f} - \delta^4\tilde{\nu}^2 - \delta^4\nabla\tilde{\nu}\cdot\nabla\rho) - \frac{\delta\tilde{E}}{\delta\rho}(\rho+\tilde{\rho})\right] \times(\dot{e}+\mathbf{u}\cdot\nabla e) - \frac{\delta\tilde{E}}{\delta\rho}\nabla\cdot\mathbf{J}_\rho - \frac{\text{El}^{-1}}{\epsilon}\mathbf{u}\cdot\nabla \cdot(2\delta^2 e\nabla\rho\otimes\nabla\rho + \delta^4 e\nabla\tilde{\nu}\otimes\nabla\rho + \delta^4 e\nabla\rho\otimes\nabla\tilde{\nu})\,dx. \tag{69}$$

By analogy with Eq. (68) we may also define the notation $\frac{\delta\tilde{E}}{\delta e}$ by

$$\frac{\delta\tilde{E}}{\delta e} := \frac{\text{El}^{-1}}{\epsilon}(\tilde{f} - \delta^4\tilde{\nu}^2 - \delta^4\nabla\tilde{\nu}\cdot\nabla\rho) - \frac{\delta\tilde{E}}{\delta\rho}(\rho+\tilde{\rho}). \tag{70}$$

It remains to evaluate the material derivative of $e$. Using Eq. (41) we may calculate

$$\dot{e} = -\frac{1}{2}B'(\psi)\nabla\psi\cdot\mathbf{u} - \frac{\epsilon^2}{2}\nabla\psi\cdot\nabla\nabla\psi\cdot\mathbf{u} - \frac{\epsilon^2}{2}\nabla\psi\cdot\nabla\mathbf{u}\cdot\nabla\psi - \left[\frac{1}{2}B'(\psi) + \frac{\epsilon^2}{2}\nabla\psi\cdot\nabla\right]\nabla\cdot\tilde{\mathbf{J}}_\psi \tag{71}$$

$$= -\mathbf{u}\cdot\nabla e - \frac{\epsilon^2}{2}\nabla\psi\otimes\nabla\psi : \nabla\mathbf{u} - \left[\frac{1}{2}B'(\psi) + \frac{\epsilon^2}{2}\nabla\psi\cdot\nabla\right]\nabla\cdot\tilde{\mathbf{J}}_\psi. \tag{72}$$

Inserting Eq. (72) into Eq. (69) yields

$$\dot{\tilde{E}}_{\rm spfc} = \int_\Omega -\frac{\delta\tilde{E}}{\delta e}\left(\frac{1}{2}B'(\psi)+\frac{\epsilon^2}{2}\nabla\psi\cdot\nabla\right)\nabla\cdot\tilde{\mathbf{J}}_\psi - \nabla\cdot\tilde{\mathbf{J}}_\rho\frac{\delta\tilde{E}}{\delta\rho} - \frac{\mathrm{El}^{-1}}{\epsilon}\mathbf{u}\cdot\nabla\cdot(2\delta^2 e\nabla\rho\otimes\nabla\rho+\delta^4 e\nabla\tilde{\nu}\otimes\nabla\rho + \delta^4 e\nabla\rho\otimes\nabla\tilde{\nu}) + \mathbf{u}\cdot\nabla\cdot\left(\frac{\epsilon^2}{2}\frac{\delta\tilde{E}}{\delta e}\nabla\psi\otimes\nabla\psi\right)dx. \tag{73}$$

Now, let us put the kinetic energy, the SPFC energy, and the surface energy together to obtain the time derivative of the total energy:

$$\dot{\tilde{E}} = -\int_\Omega \frac{1}{\mathrm{Re}}\nabla\mathbf{u}:\nabla\mathbf{u}\,dx + \int_\Omega -\left(\frac{\delta\tilde{E}}{\delta e}+\frac{2}{\epsilon}\right)\times\left[\frac{1}{2}B'(\psi)+\frac{\epsilon^2}{2}\nabla\psi\cdot\nabla\right]\nabla\cdot\tilde{\mathbf{J}}_\psi\,dx + \int_\Omega -\nabla\cdot\tilde{\mathbf{J}}_\rho\frac{\delta\tilde{E}}{\delta\rho}\,dx + \int_\Omega \mathbf{u}\cdot(\tilde{\mathbf{F}}-\nabla\cdot\mathbf{T}_{\rm sing})\,dx, \tag{74}$$

where we have introduced the singular stress tensor

$$\mathbf{T}_{\rm sing} = \frac{\mathrm{El}^{-1}}{\epsilon}e(2\delta^2\nabla\rho\otimes\nabla\rho+\delta^4\nabla\tilde{\nu}\otimes\nabla\rho+\delta^4\nabla\rho\otimes\nabla\tilde{\nu}) - \epsilon\nabla\psi\otimes\nabla\psi\left(1+\frac{\epsilon}{2}\frac{\delta\tilde{E}}{\delta e}\right). \tag{75}$$

Integrating by parts gives

$$\dot{\tilde{E}} = -\int_\Omega \frac{1}{\mathrm{Re}}\nabla\mathbf{u}:\nabla\mathbf{u}\,dx + \int_\Omega \tilde{\mathbf{J}}_\psi\cdot\nabla\left(\mu\left[\frac{\epsilon}{2}\frac{\delta\tilde{E}}{\delta e}+1\right] - \frac{\epsilon^2}{2}\nabla\frac{\delta\tilde{E}}{\delta e}\cdot\nabla\psi\right)dx + \int_\Omega \tilde{\mathbf{J}}_\rho\cdot\nabla\frac{\delta\tilde{E}}{\delta\rho}dx + \int_\Omega \mathbf{u}\cdot(\tilde{\mathbf{F}}-\nabla\cdot\mathbf{T}_{\rm sing})dx. \tag{76}$$

By taking

$$\tilde{\mathbf{F}} = \nabla\cdot\mathbf{T}_{\rm sing}, \tag{77}$$

$$\tilde{\mathbf{J}}_\psi = -\mathrm{Pe}_\psi^{-1}\epsilon B\nabla\left(\mu\left[\frac{\epsilon}{2}\frac{\delta\tilde{E}}{\delta e}+1\right]-\frac{\epsilon^2}{2}\nabla\frac{\delta\tilde{E}}{\delta e}\cdot\nabla\psi\right), \tag{78}$$

$$\tilde{\mathbf{J}}_\rho = -\mathrm{Pe}_\rho^{-1}\epsilon e\nabla\frac{\delta\tilde{E}}{\delta\rho}, \tag{79}$$

we obtain $\dot{\tilde{E}}\leqslant 0$, which ensures thermodynamic consistency.

If the flux $\tilde{\mathbf{J}}_\psi$ as defined in Eq. (78) is used in the conservation equation (41), the resulting $\psi$ does not provide a good description of the interface layer because of the contributions of $\tilde{E}_{\rm spfc}$ to the variational derivatives. To be more precise, the factor of the Cahn-Hilliard chemical potential, $\frac{\epsilon}{2}\frac{\delta\tilde{E}}{\delta e}+1$, may be negative if $\mathrm{El}^{-1}$ is large, which results in a negative Cahn-Hilliard mobility. Since the primary purpose of $\psi$ is to track the two-phase interface, we simplify $\tilde{\mathbf{J}}_\psi$ and omit the terms dependent on $\tilde{E}_{\rm spfc}$, which gives the standard Cahn-Hilliard flux

$$\tilde{\mathbf{J}}_\psi = -\mathrm{Pe}_\psi^{-1}\epsilon B(\psi)\nabla\frac{\delta E_\sigma}{\delta\psi} = -\mathrm{Pe}_\psi^{-1}\epsilon B\nabla\mu. \tag{80}$$

Although the resulting system is no longer variational and does not necessarily decrease the energy, this effect tends to be higher order since away from the interface $B(\psi)\approx 0$ and near the interface $\psi$ locally equilibrates yielding $B'(\psi)-\epsilon^2\Delta\psi\approx 0$. Note that if $\tilde{\mathbf{J}}_\psi\approx 0$, then $\dot{\tilde{E}}\leqslant 0$ with $\mathbf{F}$ and $\tilde{\mathbf{J}}_\rho$ given in Eqs. (77) and (79). In addition, we will show in Sec. V that the system we obtained above is the diffuse interface version of a thermodynamically consistent sharp interface system, and in this sense remains variational.

### B. Summary of governing equations

Putting everything together, we now summarize the new nondimensional Navier-Stokes-Cahn-Hilliard Surface-Phase-Field-Crystal (NSCHSPFC) equations. We write the equations as a system of second order partial differential equations. The advective Cahn-Hilliard equation governing the motion of the two-phase interface remains unchanged, but is repeated here for completeness:

$$\partial_t\psi + \mathbf{u}\cdot\nabla\psi = \mathrm{Pe}_\psi^{-1}\epsilon\nabla\cdot[B(\psi)\nabla\mu], \tag{81}$$

$$\mu = \epsilon^{-1}B'(\psi)-\epsilon\Delta\psi. \tag{82}$$

The new surface-phase-field-crystal equation on the diffuse interface defined by $\psi$ governs the evolution of the surface colloids:

$$\partial_t[e(\rho+\tilde{\rho})]+\nabla\cdot[e\mathbf{u}(\rho+\tilde{\rho})] = \mathrm{Pe}_\rho^{-1}\nabla\cdot(e\nabla\tilde{\omega}), \tag{83}$$

$$e\tilde{\omega} = e\rho(\rho^2+1+r)+2\delta^2 e\tilde{\nu}+\delta^4\nabla\cdot(e\nabla\tilde{\nu}), \tag{84}$$

$$e\tilde{\nu} = \nabla\cdot(e\nabla\rho). \tag{85}$$

Finally, the Navier-Stokes equations govern the motion of the fluids:

$$\partial_t\mathbf{u}+(\mathbf{u}\cdot\nabla)\mathbf{u} = -\nabla p+\frac{1}{\mathrm{Re}}\Delta\mathbf{u}+\nabla\cdot\mathbf{T}_{\rm sing}, \tag{86}$$

$$\nabla\cdot\mathbf{u} = 0, \tag{87}$$

where the surface tension and elastic force are contained in the singular stress tensor $\mathbf{T}_{\rm sing}$ defined in Eqs. (68), (70), and (75). The sixth order, nonlinear, nonlocal NSCHSPFC system is equipped with the initial conditions

$$\mathbf{u}(t=0,\mathbf{x})=\mathbf{u}_0(\mathbf{x}),\quad \psi(t=0,\mathbf{x})=\psi_0(\mathbf{x}),\quad \rho(t=0,\mathbf{x})=\rho_0(\mathbf{x}),\quad \text{in }\Omega$$

and either natural boundary conditions

$$\frac{\partial\psi}{\partial\mathbf{n}}=\frac{\partial\rho}{\partial\mathbf{n}}=\frac{\partial\mu}{\partial\mathbf{n}}=\frac{\partial\tilde{\nu}}{\partial\mathbf{n}}=\frac{\partial\tilde{\omega}}{\partial\mathbf{n}}=0,\qquad \mathbf{u}=\mathbf{u}_\infty\quad\text{on }\partial\Omega,$$

where $\mathbf{n}$ denotes the outward normal vector, or periodic boundary conditions.

### C. Evaluating the divergence of the stress tensor

In this section we will evaluate the divergence of the stress tensor $\mathbf{T}_{\rm sing}$ to obtain further insight into the force $\tilde{\mathbf{F}}$. This will enable a straightforward comparison with the sharp

interface analog given in Sec. V. Moreover, we will see that $\tilde{\mathbf{F}}$ includes the new elastic force $\mathbf{F}_{\text{new}}$. First, one may easily verify that

$$\frac{\text{El}^{-1}}{\epsilon}\nabla\cdot[e(2\delta^2\nabla\rho\otimes\nabla\rho+\delta^4\nabla\tilde{\nu}\otimes\nabla\rho+\delta^4\nabla\rho\otimes\nabla\tilde{\nu})] = e\left\{\frac{\delta\tilde{E}}{\delta\rho}\nabla\rho-\nabla\left[\frac{\delta\tilde{E}}{\delta e}+\frac{\delta\tilde{E}}{\delta\rho}(\rho+\tilde{\rho})\right]\right\} \tag{88}$$

and

$$\begin{aligned}-\nabla\cdot\left[\epsilon\nabla\psi\otimes\nabla\psi\left(1+\frac{\epsilon}{2}\frac{\delta\tilde{E}}{\delta e}\right)\right] &= -\epsilon\nabla\left(1+\frac{\epsilon}{2}\frac{\delta\tilde{E}}{\delta e}\right)\cdot\nabla\psi\otimes\nabla\psi-\epsilon\left(1+\frac{\epsilon}{2}\frac{\delta\tilde{E}}{\delta e}\right)\\ &\quad\times(\Delta\psi\nabla\psi+\nabla\psi\cdot\nabla\nabla\psi) \qquad (89)\\ &= -\epsilon\nabla\left(1+\frac{\epsilon}{2}\frac{\delta\tilde{E}}{\delta e}\right)\cdot\nabla\psi\otimes\nabla\psi+\left(1+\frac{\epsilon}{2}\frac{\delta\tilde{E}}{\delta e}\right)\\ &\quad\times\left(\mu\nabla\psi-\frac{2}{\epsilon}\nabla e\right). \qquad (90)\end{aligned}$$

Adding both gives

$$\begin{aligned}\tilde{\mathbf{F}} &= \nabla\cdot\mathbf{T}_{\text{sing}}\\ &= -\nabla\left(e\left[\frac{2}{\epsilon}+\frac{\delta\tilde{E}}{\delta e}\right]\right)-e(\rho+\tilde{\rho})\nabla\frac{\delta\tilde{E}}{\delta\rho}\\ &\quad-\frac{\epsilon^2}{2}\nabla\psi\otimes\nabla\psi\cdot\nabla\frac{\delta\tilde{E}}{\delta e}+\left(1+\frac{\epsilon}{2}\frac{\delta\tilde{E}}{\delta e}\right)\mu\nabla\psi. \qquad (91)\end{aligned}$$

The first term on the right-hand side is a gradient term and can therefore be neglected as it does not affect the flow profile (e.g., modifies the pressure). We will drop the term and note this by using equivalent ($\equiv$) instead of equal ($=$) in the following. Therefore, we have

$$\begin{aligned}\tilde{\mathbf{F}} &\equiv -e(\rho+\tilde{\rho})\nabla\frac{\delta\tilde{E}}{\delta\rho}-\frac{\epsilon^2}{2}\nabla\psi\otimes\nabla\psi\cdot\nabla\frac{\delta\tilde{E}}{\delta e}\\ &\quad+\left(1+\frac{\epsilon}{2}\frac{\delta\tilde{E}}{\delta e}\right)\mu\nabla\psi. \qquad (92)\end{aligned}$$

Now, examine $\nabla\psi\cdot\nabla\frac{\delta\tilde{E}}{\delta e}$. First, we may use that $\rho$, $\tilde{\nu}$ and $\frac{\delta\tilde{E}}{\delta\rho}$ are to highest order constant in normal direction and $\nabla\psi$ is normal to the interface. This allows the approximation

$$\begin{aligned}\nabla\psi\cdot\nabla\frac{\delta\tilde{E}}{\delta e} &\approx \frac{\text{El}^{-1}}{\epsilon}\nabla\psi\cdot\nabla(-\delta^2|\nabla\rho|^2-\delta^4\nabla\tilde{\nu}\cdot\nabla\rho) \qquad (93)\\ &= -\frac{\text{El}^{-1}}{\epsilon}(2\delta^2\nabla\psi\cdot\nabla\nabla\rho\cdot\nabla\rho+\delta^4\nabla\psi\cdot\nabla\nabla\rho\cdot\nabla\tilde{\nu}+\delta^4\nabla\psi\cdot\nabla\nabla\tilde{\nu}\cdot\nabla\rho)\\ &= -\frac{\text{El}^{-1}}{\epsilon}(2\delta^2\nabla(\nabla\psi\cdot\nabla\rho)\cdot\nabla\rho-2\delta^2\nabla\rho\cdot\nabla\nabla\psi\cdot\nabla\rho+\delta^4\nabla(\nabla\psi\cdot\nabla\rho)\cdot\nabla\tilde{\nu}+\delta^4\nabla(\nabla\psi\cdot\nabla\tilde{\nu})\cdot\nabla\rho\\ &\quad-2\delta^4\nabla\rho\cdot\nabla\nabla\psi\cdot\nabla\tilde{\nu}) \qquad (94)\\ &\approx \frac{\text{E}^{-1}}{\epsilon}(2\delta^2\nabla\rho\cdot\nabla\nabla\psi\cdot\nabla\rho+2\delta^4\nabla\rho\cdot\nabla\nabla\psi\cdot\nabla\tilde{\nu}) \qquad (95)\\ &\approx \frac{\text{El}^{-1}}{\epsilon}(2\delta^2|\nabla\rho|^2+2\delta^4\nabla\tilde{\nu}\cdot\nabla\rho)\mathbf{t}\cdot\nabla\nabla\psi\cdot\mathbf{t}, \qquad (96)\end{aligned}$$

where

$$\mathbf{t}:=\frac{\nabla\rho}{|\nabla\rho|}=\frac{\nabla\tilde{\nu}}{|\nabla\tilde{\nu}|} \tag{97}$$

denotes the unit tangent vector. From differential geometry (e.g., see Ref. [27]) it is known that

$$\mathbf{t}\cdot\nabla\nabla\psi\cdot\mathbf{t}=\kappa_{\mathbf{t}}|\nabla\psi|, \tag{98}$$

where $\kappa_{\mathbf{t}}$ is the normal curvature of the interface along $\mathbf{t}$. In the following, we will restrict ourselves to 2D, where $\kappa_{\mathbf{t}}=\kappa$. Inserting Eq. (98) into Eq. (96), we can write

$$\frac{\epsilon^2}{2}\nabla\psi\otimes\nabla\psi\cdot\nabla\frac{\delta\tilde{E}}{\delta e}\approx\frac{\text{El}^{-1}}{2}\epsilon\nabla\psi|\nabla\psi|\kappa(2\delta^2|\nabla\rho|^2+2\delta^4\nabla\tilde{\nu}\cdot\nabla\rho). \tag{99}$$

Now, we can use the fact that $\nabla\psi=\mathbf{n}|\nabla\psi|$ and that $3\sqrt{2}\epsilon|\nabla\psi|^2$ approximates the surface delta function for $\epsilon\to 0$ and deduce

$$\frac{\epsilon^2}{2}\nabla\psi\otimes\nabla\psi\cdot\nabla\frac{\delta\tilde{E}}{\delta e}\approx\frac{\text{El}^{-1}}{2}\frac{1}{3\sqrt{2}}\delta_\Gamma\kappa\mathbf{n}(2\delta^2|\nabla\rho|^2+2\delta^4\nabla\tilde{\nu}\cdot\nabla\rho). \tag{100}$$

Finally, using Eq. (32), we obtain

$$\frac{\epsilon^2}{2}\nabla\psi\otimes\nabla\psi\cdot\nabla\frac{\delta\tilde{E}}{\delta e}\approx-\frac{\text{El}^{-1}}{2}\mu\nabla\psi(2\delta^2|\nabla\rho|^2+2\delta^4\nabla\tilde{\nu}\cdot\nabla\rho). \tag{101}$$

This can be inserted into Eq. (92) to give

$$\tilde{\mathbf{F}} \approx -e(\rho+\tilde{\rho})\boldsymbol{\nabla}\frac{\delta\tilde{E}}{\delta\rho} - \frac{\epsilon}{2}\mu\boldsymbol{\nabla}\psi\frac{\delta\tilde{E}}{\delta\rho}(\rho+\tilde{\rho}) + \mu\boldsymbol{\nabla}\psi + \frac{\mathrm{El}^{-1}}{2}\mu\boldsymbol{\nabla}\psi\left(\frac{1}{4}\rho^4 + \frac{1+r}{2}\rho^2 - \frac{\delta^4}{2}\tilde{v}^2 + \delta^2|\boldsymbol{\nabla}\rho|^2 + \delta^4\boldsymbol{\nabla}\tilde{v}\cdot\boldsymbol{\nabla}\rho\right). \quad (102)$$

Examining the last term on the right-hand side, we recover the (new) elastic force $\mathbf{F}_{\text{new}}$ derived in Sec. III. Also, the third term, $\mu\boldsymbol{\nabla}\psi$, occurred in the original equations, but the first and second terms in $\tilde{\mathbf{F}}$ differ from the original NSCHSPFC model. This is due to the fact that in the derivation of the original NSCHSPFC model, the assumption of conserved dynamics led to an additional term in the Cahn-Hilliard chemical potential rather than in the force $\tilde{\mathbf{F}}$ and was dropped in the original paper, since it led to a poor description of the interface. If in the derivation of the model we had neglected the conservation of $\rho+\tilde{\rho}$ as well, that is, if we had assumed $\rho$ was conserved instead of $\rho_c = \rho+\tilde{\rho}$, we would have obtained $\tilde{\mathbf{F}} \approx e\frac{\delta\tilde{E}}{\delta\rho}\boldsymbol{\nabla}\rho + \mu\boldsymbol{\nabla}\psi + \frac{\mathrm{El}^{-1}}{2}\mu\boldsymbol{\nabla}\psi(\frac{1}{4}\rho^4 + \frac{1+r}{2}\rho^2 - \frac{\delta^4}{2}\tilde{v}^2 + \delta^2|\boldsymbol{\nabla}\rho|^2 + \delta^4\boldsymbol{\nabla}\tilde{v}\cdot\boldsymbol{\nabla}\rho)$, which is the exact same force as derived in the previous section, with $B$ replaced by $e$.

To sum up, the new NSCHSPFC model presented in this section is in two dimensions equivalent to the original model equipped with the new elastic force and additional terms to account for the conservation of $\rho+\tilde{\rho}$. In the next section we validate the model by demonstrating that the NSCHSPFC model is a diffuse interface approximation of a thermodynamically consistent sharp interface model.

## V. SHARP INTERFACE MODEL

In this section we derive a 2D sharp interface version of the NSCHSPFC model which we call Navier-Stokes surface-phase-field-crystal (NSSPFC) model. A similar derivation can be done in three dimensions, but involves more complicated differential geometry (e.g., see Ref. [28]), where the variational derivatives of the sharp interface surface PFC energy are computed. For the derivation here we use a one-dimensional parametrization of the interface, and we demonstrate that the NSCHSPFC model derived in the previous section is a diffuse interface approximation of the NSSPFC model.

### A. Derivation of a sharp interface model

In the following let us denote the arc length by $s$ and the derivative along the interface with subscript $s$. We derive the NSSPFC model following the ideas in Ref. [15] but replacing the total energy $E$ with its sharp interface analog

$$\bar{E} = \bar{E}_{\text{spfc}} + \bar{E}_\sigma + E_{\text{kin}}, \quad (103)$$

where

$$\bar{E}_{\text{spfc}} = \frac{\mathrm{El}^{-1}}{6\sqrt{2}}\int_\Gamma \bar{f}\,ds, \quad (104)$$

with

$$\bar{f} = \frac{1}{4}\rho^4 + \frac{1+r}{2}\rho^2 - \delta^2\rho_s^2 + \frac{\delta^4}{2}\rho_{ss}^2 \quad (105)$$

and

$$\bar{E}_\sigma = \int_\Gamma \frac{1}{3\sqrt{2}}\,ds \quad (106)$$

are the sharp interface versions of $E_{\text{spfc}}$ and $E_\sigma$, respectively. The factors $6\sqrt{2}$ and $3\sqrt{2}$ arise to match the scaling according to Eqs. (4) and (8). Now, we can parametrize the interface with a real-valued parameter $\alpha \in [0,1]$ and write

$$\bar{E} = \frac{\mathrm{El}^{-1}}{6\sqrt{2}}\int_0^1 \bar{f}s_\alpha\,d\alpha + \int_0^1 \frac{1}{3\sqrt{2}}s_\alpha\,d\alpha + E_{\text{kin}}. \quad (107)$$

To vary $\Gamma$ and $\rho$ we take the time derivative of $\bar{E}$,

$$\frac{d}{dt}\bar{E} = \frac{\mathrm{El}^{-1}}{6\sqrt{2}}\int_0^1 \dot{\bar{f}}s_\alpha + \bar{f}\partial_t s_\alpha\,d\alpha + \int_0^1 \frac{1}{3\sqrt{2}}\partial_t s_\alpha\,d\alpha + \frac{d}{dt}E_{\text{kin}}, \quad (108)$$

where the overdot denotes the material derivative $\partial_t + \mathbf{u}\cdot\boldsymbol{\nabla}$. Now, we can use that

$$\partial_t s_\alpha = s_\alpha(T_s + \kappa V), \quad (109)$$

where $T$ is the tangential and $V$ the normal velocity. We get

$$\begin{aligned}\frac{d}{dt}\bar{E} &= \int_0^1 \frac{\mathrm{El}^{-1}}{6\sqrt{2}}[\dot{\bar{f}}s_\alpha + \bar{f}s_\alpha(T_s+\kappa V)] + \frac{1}{3\sqrt{2}}s_\alpha(T_s+\kappa V)\,d\alpha + \frac{d}{dt}E_{\text{kin}} \\ &= \int_\Gamma \frac{\mathrm{El}^{-1}}{6\sqrt{2}}[\dot{\bar{f}} + \bar{f}(T_s+\kappa V)] + \frac{1}{3\sqrt{2}}\kappa V\,ds + \frac{d}{dt}E_{\text{kin}}.\end{aligned} \quad (110)$$

Furthermore, we compute

$$\begin{aligned}\int_\Gamma \dot{\bar{f}}\,ds &= \int_\Gamma [\rho^3 + (1+r)\rho]\dot{\rho} - 2\delta^2\rho_s\left(\frac{1}{s_\alpha}\rho_\alpha\right)^{\cdot} + \delta^4\rho_{ss}\left[\frac{1}{s_\alpha}\left(\frac{1}{s_\alpha}\rho_\alpha\right)_\alpha\right]^{\cdot} ds \\ &= \int_\Gamma [\rho^3 + (1+r)\rho]\dot{\rho} - 2\delta^2\rho_s\dot{\rho}_s + 2\delta^2\rho_s\frac{\partial_t s_\alpha}{s_\alpha}\rho_s - \delta^4\rho_{ss}\left(\frac{\partial_t s_\alpha}{s_\alpha}\rho_{ss}\right) \\ &\quad + \delta^4\rho_{ss}\left(\frac{\partial_t s_\alpha}{s_\alpha}\rho_s\right)_s + \delta^4\rho_{ss}(\dot{\rho})_{ss}\,ds \\ &= \int_\Gamma \dot{\rho}\left[\rho^3 + (1+r)\rho + 2\delta^2\rho_{ss} + \delta^4\rho_{ssss}\right] + \frac{\partial_t s_\alpha}{s_\alpha}\left(2\delta^2\rho_s^2 - \delta^4\rho_{ss}^2 + \delta^4\rho_{sss}\rho_s\right) ds.\end{aligned} \quad (111)$$

Now, let us define

$$\frac{\delta\bar{E}}{\delta\rho} = \frac{\mathrm{El}^{-1}}{6\sqrt{2}}[\rho^3 + (1+r)\rho + 2\delta^2\rho_{ss} + \delta^4\rho_{ssss}] \quad (112)$$

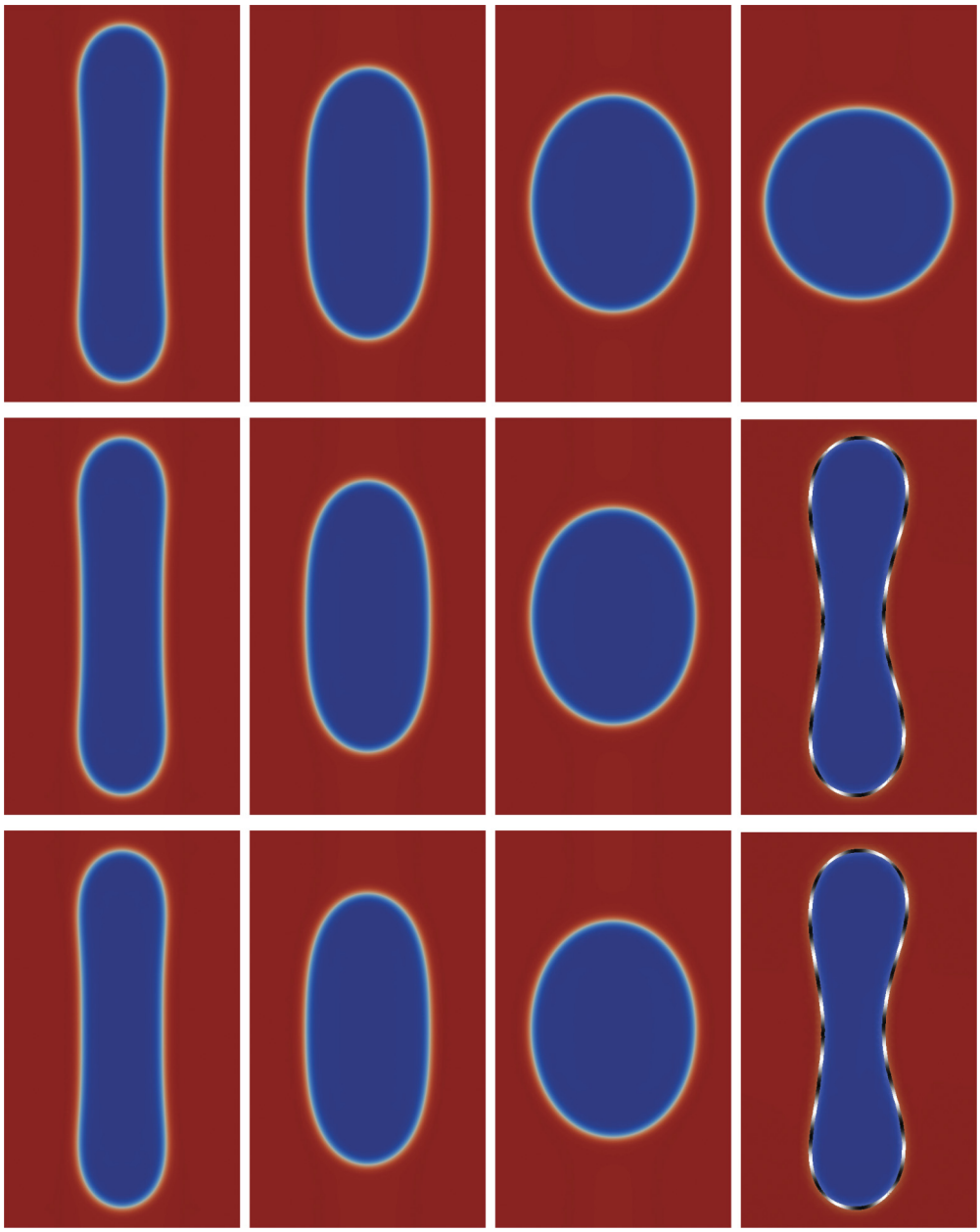

FIG. 2. (Color online) Retraction of an elliptical drop without colloidal forces (top row), with the old elastic force (middle row) and with the new elastic force (bottom row) at times $t = 0, 33, 67, 1671$, from left to right. The drop and matrix fluids have different shades, lighter (red) for $\psi = 1$ and darker (blue) for $\psi = 0$. The colloids ($\rho$) on the interface are colored black ($\rho < 0$) and white ($\rho > 0$).

and

$$\bar{g} := \bar{f} + 2\delta^2 \rho_s^2 - \delta^4 \rho_{ss}^2 + \delta^4 \rho_{sss} \rho_s. \tag{113}$$

From Eqs. (109)–(111) we obtain

$$\begin{aligned} \frac{d}{dt}\bar{E} &= \int_\Gamma \dot{\rho} \frac{\delta \bar{E}}{\delta \rho} + \frac{\mathrm{El}^{-1}}{6\sqrt{2}}(T_s + \kappa V) g \, ds + \int_\Gamma \frac{1}{3\sqrt{2}} \kappa V \, ds + \frac{d}{dt} E_{\mathrm{kin}} = \int_\Gamma \dot{\rho} \frac{\delta \bar{E}}{\delta \rho} + \frac{\mathrm{El}^{-1}}{6\sqrt{2}} (\kappa V g - T g_s) \, ds \\ &+ \int_\Gamma \frac{1}{3\sqrt{2}} \kappa V \, ds + \frac{d}{dt} E_{\mathrm{kin}} = \int_\Gamma \dot{\rho} \frac{\delta \bar{E}}{\delta \rho} + \frac{\mathrm{El}^{-1}}{6\sqrt{2}} \kappa V g - T \frac{\delta \bar{E}}{\delta \rho} \rho_s \, ds + \int_\Gamma \frac{1}{3\sqrt{2}} \kappa V \, ds + \frac{d}{dt} E_{\mathrm{kin}}. \end{aligned} \tag{114}$$

Now, we can use that $\frac{d}{dt} E_{\mathrm{kin}} = \int_\Omega \mathbf{u} \cdot \partial_t \mathbf{u} \, dx$ and suppose that the fluid motion is governed by the Navier-Stokes equation, which in nondimensional form is given by

$$\partial_t \mathbf{u} = -\mathbf{u} \cdot \boldsymbol{\nabla} \mathbf{u} - \boldsymbol{\nabla} p + \frac{1}{\mathrm{Re}} \Delta \mathbf{u} + \bar{\mathbf{F}}, \quad \boldsymbol{\nabla} \cdot \mathbf{u} = 0 \quad \text{in } \Omega. \tag{115}$$

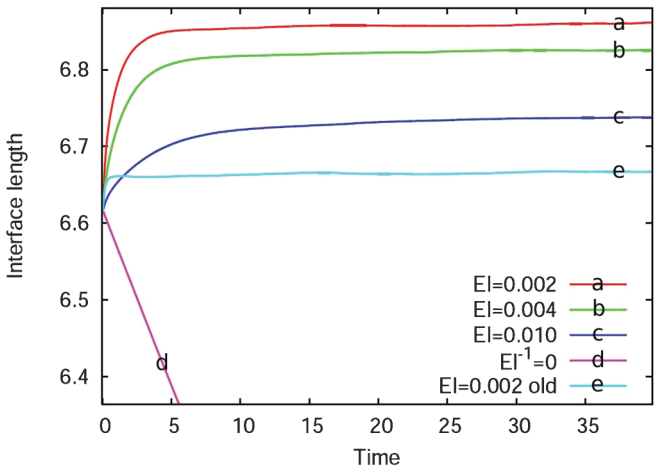


FIG. 3. (Color online) The interface length versus time for the new elastic force formulation for different strengths of elastic forces (a)–(d), and for the old elastic force for El = 0.002 (e), for the simulations presented in Fig. 2.

The force $\bar{\mathbf{F}}$ is as yet unspecified. Furthermore, we assume the evolution of $\rho$ as

$$\dot{\rho} = -\nabla_\Gamma \cdot T(\rho+\tilde{\rho}) - (\rho+\tilde{\rho})\kappa V - \nabla_\Gamma \cdot \bar{\mathbf{J}}_\rho \quad \text{on } \Gamma, \quad (116)$$

which ensures conservation of $\rho+\tilde{\rho}$. Also the flux $\bar{\mathbf{J}}_\rho$ has not yet been specified. Now, we can insert Eqs. (115) and (116) into Eq. (114). The time derivative of the energy becomes

$$\begin{aligned}\frac{d}{dt}\bar{E} &= \int_\Omega -\frac{1}{\mathrm{Re}}\nabla\mathbf{u} : \nabla\mathbf{u} + \mathbf{u}\cdot\bar{\mathbf{F}}\,dx + \int_\Gamma \bar{\mathbf{J}}_\rho \nabla_\Gamma \frac{\delta\bar{E}}{\delta\rho}\,ds \\ &\quad + \int_\Gamma \frac{\mathrm{El}^{-1}}{6\sqrt{2}}\kappa V g + \frac{1}{3\sqrt{2}}\kappa V - \kappa V(\rho+\tilde{\rho})\frac{\delta\bar{E}}{\delta\rho} \\ &\quad + T(\rho+\tilde{\rho})\nabla_\Gamma\frac{\delta\bar{E}}{\delta\rho}\,ds \\ &= -\frac{1}{\mathrm{Re}}\int_\Omega \nabla\mathbf{u} : \nabla\mathbf{u}\,dx + \int_\Gamma \bar{\mathbf{J}}_\rho\nabla_\Gamma\frac{\delta\bar{E}}{\delta\rho}\,ds \\ &\quad + \int_\Omega \mathbf{u}\cdot\left\{\bar{\mathbf{F}} + \delta_\Gamma\left[\frac{\mathrm{El}^{-1}}{6\sqrt{2}}\kappa\mathbf{n}g + \frac{1}{3\sqrt{2}}\kappa\mathbf{n}\right.\right. \\ &\quad \left.\left. - \kappa\mathbf{n}(\rho+\tilde{\rho})\frac{\delta\bar{E}}{\delta\rho} + (\rho+\tilde{\rho})\nabla_\Gamma\frac{\delta\bar{E}}{\delta\rho}\right]\right\}dx.\end{aligned}$$

Hence, we obtain decreasing energy, $\dot{\bar{E}} \leqslant 0$, by taking

$$\begin{aligned}\bar{\mathbf{F}} &= -\frac{\mathrm{El}^{-1}}{6\sqrt{2}}\delta_\Gamma\kappa\mathbf{n}g - \frac{1}{3\sqrt{2}}\delta_\Gamma\kappa\mathbf{n} + \delta_\Gamma\kappa\mathbf{n}\frac{\delta\bar{E}}{\delta\rho}(\rho+\tilde{\rho}) \\ &\quad - \delta_\Gamma(\rho+\tilde{\rho})\nabla_\Gamma\frac{\delta\bar{E}}{\delta\rho}, \quad (117)\end{aligned}$$

$$\bar{\mathbf{J}}_\rho = -6\sqrt{2}\mathrm{Pe}_\rho^{-1}\nabla_\Gamma\frac{\delta E}{\delta\rho}. \quad (118)$$

Now, the resulting governing equations for the sharp interface NSSPFC model are Eqs. (115) and (116) with $\bar{\mathbf{F}}$ and $\bar{\mathbf{J}}_\rho$ from Eqs. (117) and (118).

We can obtain a diffuse interface approximation for $\bar{\mathbf{F}}$ by using Eqs. (3) and (32) to approximate $\delta_\Gamma$ and $\delta_\Gamma\kappa\mathbf{n}$, respectively. Doing so, we recover the force $\tilde{\mathbf{F}}$ from Eq. (102) derived in the previous section with the identifications $\nabla\rho \to \rho_s$, $\tilde{\nu} \to \rho_{ss}$ and $\nabla\tilde{\nu} \to \rho_{sss}$. Furthermore, with $\bar{\mathbf{J}}_\rho$ chosen as in Eq. (118) the evolution equation for $\rho$ matches exactly its diffuse interface analog given in Eq. (42). In this sense, the NSCHSPFC system given in Sec. IV is the diffuse interface version of the thermodynamically consistent sharp interface model (115)–(118) and its generalization to three dimensions.

## VI. NUMERICAL METHODS

An adaptive finite element method is used to solve the sixth order nonlinear, nonlocal system of Eqs. (81)–(87);

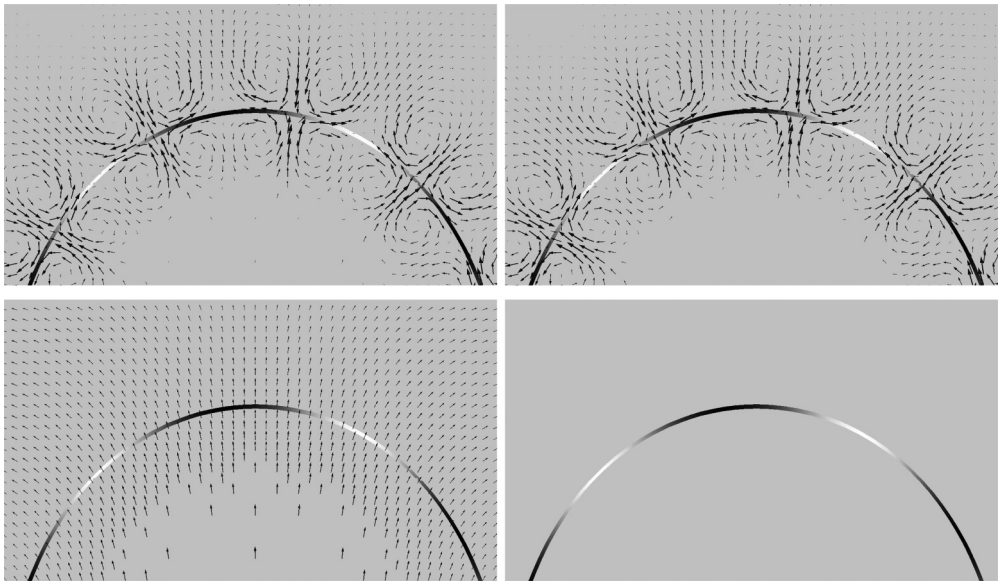

FIG. 4. Velocity field at the top of the ellipse for the old (top) and new (bottom) formulation of the elastic force at the early time $t = 0.5$ (left) and at $t = 5.0$ (right). The black-white line indicates the interface position and the location of the colloids. The arrow length indicates the velocity magnitude, for the new formulation at $t = 5.0$ (bottom right) the arrows are too small to be seen.

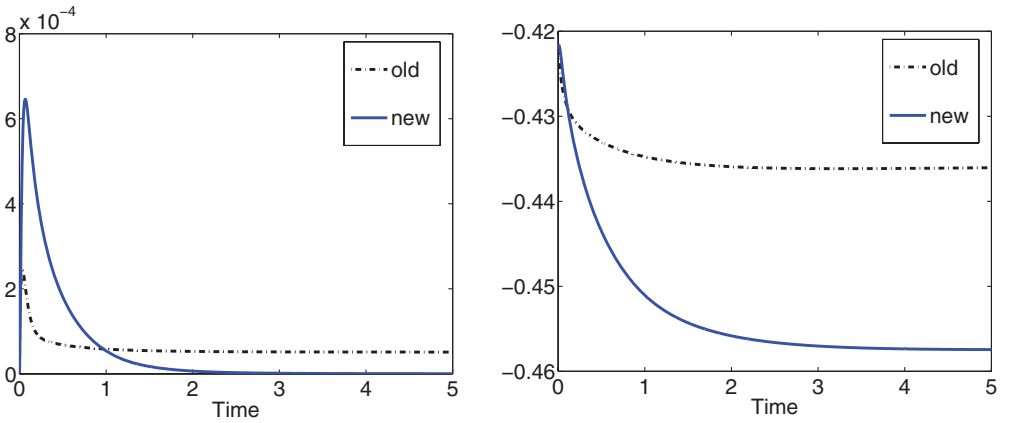


FIG. 5. (Color online) The kinetic energy (left) and total energy (right) over time for the simulations shown in Fig. 2.

the method is implemented using the adaptive finite element toolbox AMDiS [29]. We solve the coupled system as follows. First the Cahn-Hilliard equations (81) and (82) are solved to determine the position of the interface, then the SPFC equations (83)–(85) are solved to determine the surface colloid particle density. Finally the Navier-Stokes equations (87) and (86) are solved to determine the fluid velocity using the new position of the interface and the surface particle density of the colloids in the surface tension and elastic forces. To ensure the well-posedness of Eqs. (83)–(85), $e$ is replaced by $e+\xi$ (see Ref. [25], for example), with $\xi = 10^{-6}$.

A semi-implicit Euler method is used for the time discretization keeping as many terms implicit as possible. Nonlinear terms are linearized by a Taylor expansion dropping terms of order two and higher so that the equations are linear at the implicit time step. In two dimensions the linearized system is solved using the direct unsymmetric multifrontal method (UMFPACK [30]). For the 3D simulations we use an MPI-based parallelization with 64 cores and a PETSc solver TFQMR (transpose-free quasiminimal residual) with the block Jacobi preconditioner. The local subproblems are solved using incomplete LU factorization [31].

We use linear basis functions for all variables. Accordingly, the Cahn-Hilliard and SPFC equations are solved as coupled systems of second order equations (e.g., see Refs. [32,33]). The Navier-Stokes equations are solved using a first order projection method given by

$$\frac{\mathbf{u}^* - \mathbf{u}^{m-1}}{\tau} - \eta\Delta\mathbf{u}^* + \mathbf{u}^{m-1}\cdot\nabla\mathbf{u}^* + \nabla p^{m-1} = \tilde{\mathbf{F}}^m, \quad (119)$$

$$\tau\Delta p^* = \nabla\cdot\mathbf{u}^*, \quad (120)$$

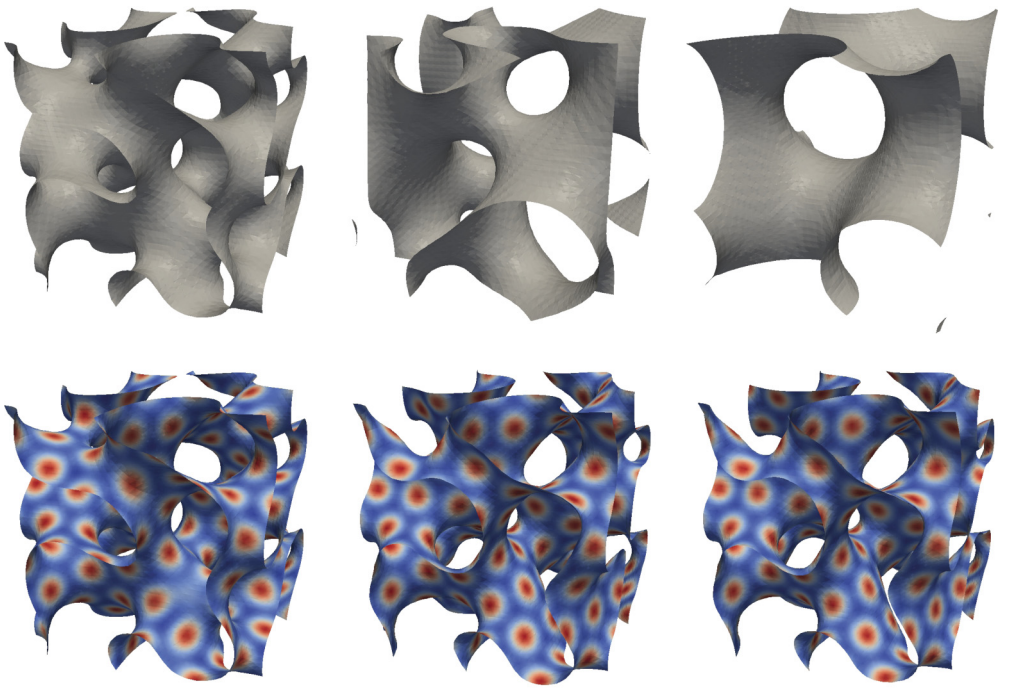

FIG. 6. (Color online) Coarsening of a fluid structure after spinodal decomposition without (top) and with (bottom) colloidal forces at times $t = 0, 134, 267$.

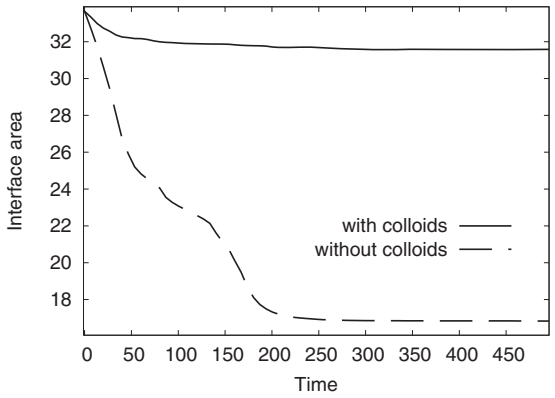


FIG. 7. The interface area versus time for the case with and without colloids.

$$\mathbf{u}^m = \mathbf{u}^* - \tau \boldsymbol{\nabla} p^*, \tag{121}$$

$$p^m = p^{m+1} + p^*, \tag{122}$$

where $\tau$ denotes the time step and the superscripts denote the time iteration.

Adaptive mesh refinement is indispensable for providing a high spatial resolution along the fluid-fluid interfaces described implicitly by $\psi$. For local mesh adaptation, we use a $L^2$-like error indicator based on a jump residual (e.g., see Refs. [29,34]) for $\psi$ to maintain approximately five grid points across the transition layers. Although we did not find it necessary to do here, additional mesh refinement can be used to increase local resolution of the flow field (e.g., velocity gradients, etc.).

## VII. RESULTS

### A. Retracting ellipse

As a first test for the NSCHSPFC model we consider the case of an initially elliptical fluid droplet surrounded by another fluid. The test setup and parameters are the same as in Ref. [15], but repeated here for completeness. The computational domain is $\Omega = [-2,2] \times [-2,2]$. We start with an initial condition as in Eq. (1) using

$$d = 1.0 - \sqrt{\left(\frac{x}{0.35}\right)^2 + \left(\frac{y}{1.8}\right)^2}.$$

Since this $d$ is only an approximation to a signed distance function of an ellipse, we refine the initial condition by solving the Cahn-Hilliard equations (81) and (82) for a short time with velocity $\mathbf{u} = 0$ to obtain better approximation of Eq. (1). The resulting $\psi$ is the initial condition $\psi_0$ for the following simulations. It describes an elliptical drop with a vertical diameter of about 3 and a horizontal thickness of around 0.75.

To obtain an initial condition for $\rho$ we solve the SPFC equations (83)–(85) with $\tilde{\rho} = 0$ on the fixed interface defined by $\psi_0$ (e.g., $\mathbf{u}$ is set to zero). We use as an initial condition for $\rho$, a constant value of $-0.3$ plus a uniformly distributed random perturbation between $[-0.05,0.05]$ at each node. Hereafter, we write such a condition as $\rho_0 = -0.3 \pm 0.05$. Since this surface density is in the crystal phase of the PFC, the colloidal particles become ordered and arrange in a crystal-like state. We stop solving the SPFC equations when a stationary state of colloid particle density is reached. The solution $\rho$ is taken as the initial condition $\rho_0$ for the full NSCHSPFC system. Note that a single colloid corresponds to the combination of one darker region ($\rho < 0$) and one lighter region ($\rho > 0$).

The remaining parameters are chosen as follows: $\tau = 1.67 \times 10^{-3}$, $r = -0.4$, $\mathrm{Pe}_\rho = 3.76$, $\mathrm{Pe}_\psi = 0.47$, $\mathrm{Re} = 0.38$, $\mathrm{El} = 0.002$, $\epsilon = 0.03$, $\delta = 0.067$, and the fluid is initially quiescent (e.g., $\mathbf{u} = 0$ at time $t = 0$). The natural boundary conditions with $\mathbf{u}_\infty = \mathbf{0}$ are used.

Figure 2 shows the simulation without colloids ($\mathrm{El}^{-1} = 0$, top row), with the old elastic force (middle row), and with the new elastic force (bottom row). When no colloids are present the surface tension makes the ellipse retract to become circular. The presence of colloids stops the retraction by the elastic force as the colloids jam at the interface, generating a strong elastic force, and the interface crystallizes. This occurs using both the old and new forms of the elastic force. Driven by the new force, the ellipse starts to develop a neck in the middle, similar to results for elastic membranes. Such results are observed for a Helfrich model with a bending energy under the constraint of local inextensibility (see, e.g., Ref. [35]). The jamming of the colloidal particles in our model effectively leads to such

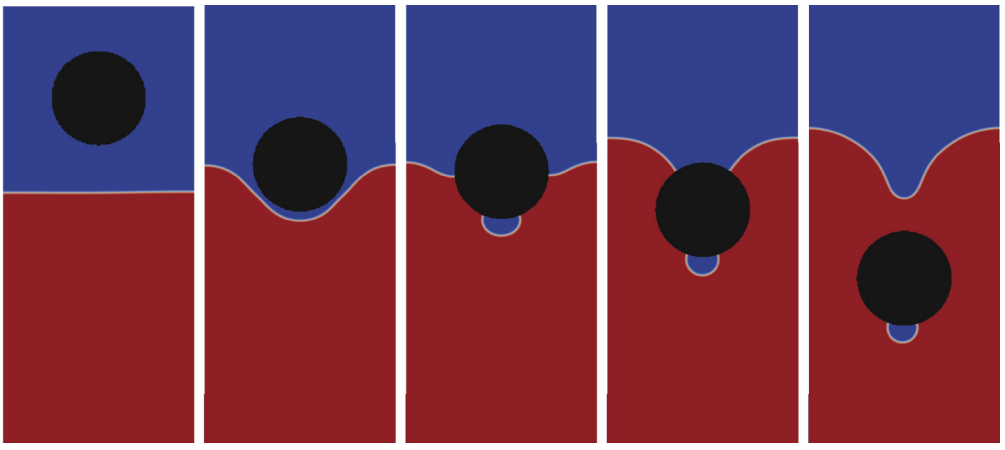

FIG. 8. (Color online) The fall of a solid ball through a fluid-fluid interface without colloids at times $t = 0$, 224, 254, 401, 685.

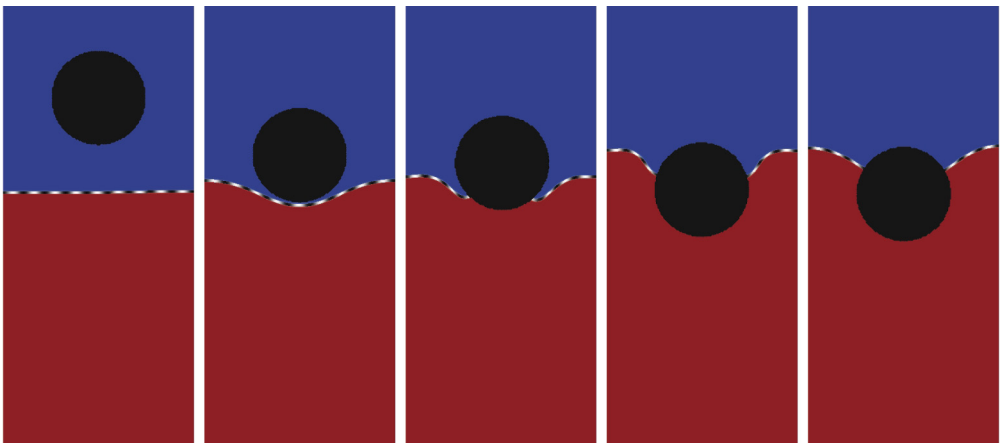

FIG. 9. (Color online) The fall of a solid ball through a fluid-fluid interface with colloids and low elasticity (El = 0.01). Images correspond to the same times as Fig. 8.

a constraint and the elastic force resulting from the particle interactions might be interpreted as a microscopic origin of the bending energy. These interpretations provide further support for the use of the new forcing term.

In Fig. 3 the interface length, calculated by the length of the $\psi = 0.5$ contour, is plotted as a function of time for different strengths of elastic forces. Initially the particles are slightly overcompressed, which results in a slight expansion of the elliptical drop. When the elasticity increases (El decreases), this effect increases and the particles can better counteract the surface tension. Furthermore, the old and new formulation of the elastic force lead to different final interface lengths [Figs. 3(a) and 3(e)].

The velocity $\mathbf{u}$ at the top of the ellipse at early times is shown in Fig. 4. For the previous model, the elastic force induces local straining flows around the interface (two per colloid), which restricts the numerical simulations to relatively small time steps and a very fine grid in a neighborhood of the interface. With the new model the straining flows seems to vanish and the velocity is much smoother.

Another nonphysical behavior of the old model is the achievement of a stable, almost stationary state with nonzero velocity. This is a characteristic feature of spurious currents (e.g., Ref. [36]). Figure 5 (left) shows the kinetic energy of the system as a measure for the total magnitude of the velocity. For the previous model $E_{\text{kin}}$ reaches a plateau above zero, whereas with the new model $E_{\text{kin}}$ seems to converge to zero over time. Also the total energy (Fig. 5, right) is decreased significantly more when $\mathbf{F}_{\text{new}}$ is used instead of $\mathbf{F}_{\text{el}}$.

### B. Jamming spinodal decomposition

A significant benefit of the new formulation is that it requires much less computational power and therefore enables 3D simulations to be performed. Next, we investigate the potential of colloidal particles to stabilize bicontinuous structures generated by spinodal decomposition. The computational domain is $\Omega = [0,8/3]^3$. As initial condition, we first generate fluid structures via spinodal decomposition by solving the CH equation in the absence of flow ($\mathbf{u} = 0$) using the initial condition $\psi = 0.5 \pm 0.1$ with a large interface thickness $\epsilon = 0.1$ for a few time steps. Then, to generate the initial condition for the full NSCHSPFC system, the CH and SPFC equations are solved together for several more time steps, again in the absence of flow, with $\epsilon = 0.03$ to refine the interface thickness and to create the colloid structure on the complex interface. As

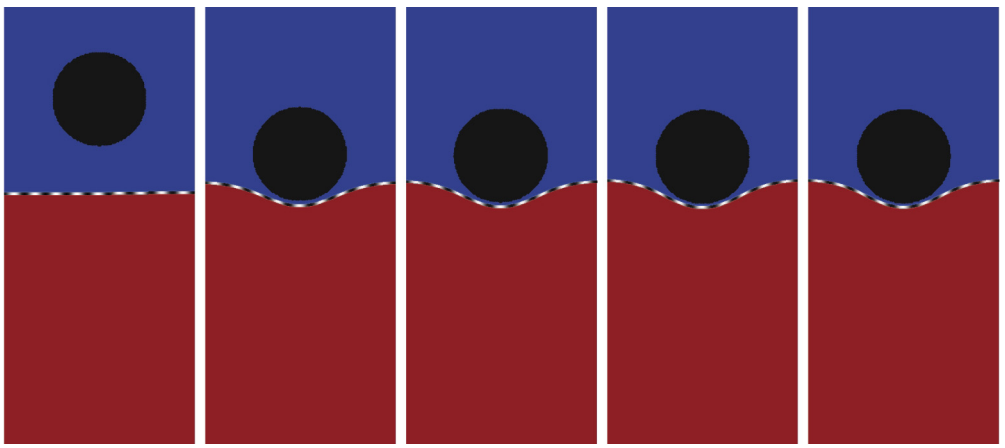

FIG. 10. (Color online) The fall of a solid ball through a fluid-fluid interface with colloids and high elasticity (El = 0.002). Images correspond to the same times as Fig. 8.

initial data for the CHSPFC solver, the previously generated $\psi$ is used together with the colloid density $\rho_0 = -0.3 \pm 0.05$. The resulting $\psi, \rho$ are used as the initial condition $\psi_0, \rho_0$ for the full NSCHSPFC system. Taking $\tau = 6.7 \times 10^{-2}$, $\mathrm{Pe}_\psi = 0.23$, $\mathrm{El} = 0.005$, and $\tilde{\rho} = 0.3$, with all other parameters as in Sec. VII A, the simulations are performed with periodic boundary conditions in each coordinate direction.

Figure 6 shows a comparison between the NSCHSPFC model (bottom) and a NSCH model without colloidal forces ($\mathrm{El}^{-1} = 0$, top). In the latter case the structure coarsens significantly. When colloids are present, the elastic force induced by the particles is able to prevent the coarsening as the colloids jam and the interface crystallizes. The interface area as a function of time time is plotted in Fig. 7.

### C. A ball falling into a fluid structure

Finally, we demonstrate a significant advantage of the multiscale NSCHSPFC model: The possibility of incorporating additional macroscopic effects. We model a solid ball, under the influence of gravity, falling through a colloid crystallized surface. This involves (1) solving the NSCHSPFC model only in $\Omega \backslash \Omega_{\mathrm{ball}}$ and (2) moving the ball with a velocity that takes into account all the forces acting on the ball. For the first part we can apply a diffuse domain approach as done in Refs. [32,37]. We therefore define a ball of radius 1 by a phase field $\phi$ using Eq. (1) with

$$d = 1.0 - \sqrt{(x - x_0)^2 + (y - y_0)^2}. \tag{123}$$

Here $(x_0, y_0)$ denotes the coordinate of the ball's center. Using the diffuse domain approach we can now formulate the NSCHSPFC model in the domain where $\{\phi \approx 1\}$: The advective Cahn-Hilliard equation becomes

$$\phi(\partial_t \psi + \mathbf{u} \cdot \nabla \psi) = \mathrm{Pe}_\psi^{-1} \epsilon \nabla \cdot (\phi B(\psi) \nabla \mu), \tag{124}$$

$$\phi \mu = \epsilon^{-1} \phi B'(\psi) - \epsilon \nabla \cdot (\phi \nabla \psi). \tag{125}$$

Note that this formulation imposes a contact angle of 90° between the fluid-fluid interface and the solid ball. The diffuse domain surface-phase-field-crystal equation is[1]

$$\partial_t [e\phi(\rho + \tilde{\rho})] + \nabla \cdot [e\phi \mathbf{u}(\rho + \tilde{\rho})] = \mathrm{Pe}_\rho^{-1} \nabla \cdot (e\phi \nabla \tilde{\omega}), \tag{126}$$

$$e\phi\tilde{\omega} = e\phi\rho(\rho^2 + 1 + r) + 2\delta^2 e\phi\tilde{\nu} + \delta^4 \nabla \cdot (e\phi \nabla \tilde{\nu}), \tag{127}$$

$$e\phi\tilde{\nu} = \nabla \cdot (e\phi \nabla \rho). \tag{128}$$

Finally, the Navier-Stokes equation becomes

$$\phi(\partial_t \mathbf{u} + (\mathbf{u} \cdot \nabla)\mathbf{u}) = -\phi \nabla a p + \frac{1}{\mathrm{Re}} \nabla \cdot (\phi \nabla \mathbf{u}) + \nabla \cdot (\phi \mathbf{T}_{\mathrm{sing}}), \tag{129}$$

$$\nabla \cdot (\phi \mathbf{u}) = \mathbf{v} \cdot \nabla \phi, \tag{130}$$

[1]This equation is derived variationally by restricting the total energy to the diffuse domain marked by $\phi \approx 1$, and then restricting the energy to the surface using $e$.

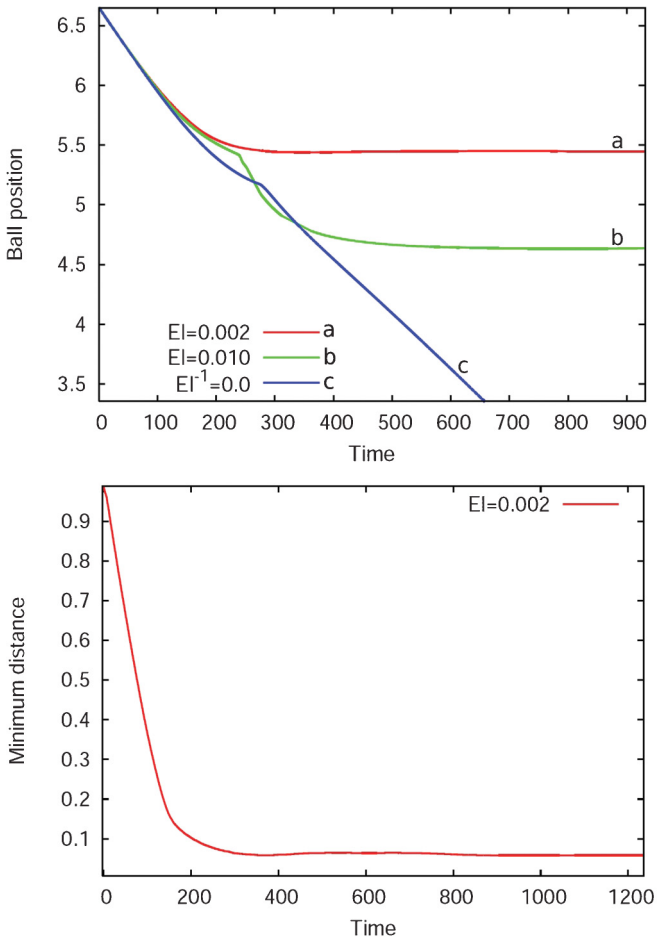


FIG. 11. (Color online) (a) The vertical position of the center of the ball over time for different strengths of elastic forces. (b) The distance minimum distance between the ball and interface when $\mathrm{El} = 0.002$.

where $\mathbf{v}$ is the velocity of the moving ball. To obtain the ball velocity we solve Newton's equation, which in nondimensional form, reads

$$\dot{\mathbf{v}} = \left( \frac{\rho_{\mathrm{fluid}}}{\rho_{\mathrm{ball}}} - 1 \right) \mathbf{g} + \frac{\rho_{\mathrm{fluid}}}{V \rho_{\mathrm{ball}}} \int_{\partial \Omega_{\mathrm{ball}}} \mathbf{T} \cdot \mathbf{n} dA, \tag{131}$$

where $\rho_{\mathrm{ball}}$ is the physical density of the ball, $V$ the nondimensional ball volume, $\mathbf{g}$ the nondimensional gravity force, and

$$\mathbf{T} := -p\mathbf{I} + \frac{1}{\mathrm{Re}} (\nabla \mathbf{u} + \nabla \mathbf{u}^T) + \mathbf{T}_{\mathrm{sing}} \tag{132}$$

the nondimensional total stress tensor, with $\mathbf{T}_{\mathrm{sing}}$ from Eq. (75). We can approximate Eq. (131) by

$$\dot{\mathbf{v}} = \left( \frac{\rho_{\mathrm{fluid}}}{\rho_{\mathrm{ball}}} - 1 \right) \mathbf{g} + \frac{\rho_{\mathrm{fluid}}}{V \rho_{\mathrm{ball}}} \int_{\Omega} \mathbf{T} \cdot \nabla \phi \, dx. \tag{133}$$

Finally, we can calculate the new ball coordinates at any time step $m$ by $(x_0, y_0)^m = (x_0, y_0)^{m-1} + \tau \mathbf{v}$, and then compute the new ball phase field $\phi$ according to Eq. (123).

The simulation is performed in $\Omega = [-2,2] \times [0,12]$. We define $\psi$ so that there is a single horizontal fluid-fluid interface at $y = 6\frac{2}{3}$ (see Fig. 8). The initial condition for $\rho$ is created

as in the previous sections. We set the ball's center initially at $[x_0(0), y_0(0)] = (0, 8\frac{2}{3})$, the initial ball velocity is set to zero. Furthermore, we use $\rho_{\text{ball}} = 2\rho_{\text{fluid}}$, $\tau = 0.033$, $\epsilon = 0.04$, $\text{Pe}_\psi = 1.88$, and $\mathbf{g} = (0, -0.48)$. Simulations are carried out once without colloids ($\text{El}^{-1} = 0$, Fig. 8), once with little elastic colloid interaction ($\text{El} = 0.01$, Fig. 9) and once with stronger colloid interaction ($\text{El} = 0.002$, Fig. 10). The remaining parameters and boundary conditions are as in Sec. VII A.

In the case when no colloids are present the ball pushes the interface downwards, then penetrates it and falls right through it. A little droplet of the upper (blue) fluid adheres to the ball, where we observe the prescribed contact angle of 90°. The presence of colloids makes the interface stiffer. In the case of a small amount of elasticity ($\text{El} = 0.01$) the interface deforms significantly less before the ball touches it. As the ball penetrates into the crystallized interface some colloids are pushed out and the ball loses speed. Finally, the ball stops falling and is trapped at the interface, despite gravity, held by the colloid-induced elastic forces. When the elastic interactions are stronger ($\text{El} = 0.002$) the ball does not even penetrate the interface. Here, the interface behaves like a solid and the ball reaches a steady position right above the interface and seems to be held by lubrication forces. Figure 11(a) shows the position of the ball over time for the three test cases, and Fig. 11(b) shows the minimum distance between the ball and interface when $\text{El} = 0.002$.

## VIII. CONCLUSIONS

In this paper we have reconsidered a model we previously developed to simulate the presence of colloids in a system with two immiscible fluid components. The model combines the NSCH equations for the two-component system with the surface PFC equations for the colloids at the interface. In particular, colloid interactions introduce elastic forces at the interface. In this paper we have introduced a new form for the elastic forces that largely eliminates spurious currents, making the system more accurate and stable to simulate. This makes 3D simulations feasible.

We derived the new elastic force in three ways. First, the old elastic force from Ref. [15] is regularized in two dimensions by averaging across the interface. Second, the elastic force is derived using an energy variation approach with a different approximation of the surface delta function than in Ref. [15]. The latter derivation is valid in two and three dimensions. If restricted to two dimensions, this leads to the same model as the previous approach. Third, a sharp interface derivation using an energy variation approach is presented in two dimensions. We show that the new formulation is the diffuse interface analog of the sharp interface model. Although we did not present the results here, we have considered another approximation of the surface delta function that contains only the gradient term in Eq. (35), scaled by a factor of two, and found results similar to those presented here. This suggests that to eliminate spurious numerical effects and to obtain a more physical solution of the problem, gradient terms should be included in the approximation of the surface delta function.

An adaptive finite element method is used to solve the new diffuse interface model numerically. We demonstrated that the new model suppresses spurious velocities and that it decreases the total energy of the system significantly more than the model derived in Ref. [15]. In two different test scenarios we show that as colloids jam on the interface and the interface crystallizes, the elastic force becomes strong enough to make the interface sufficiently rigid to resist surface tension induced coarsening. This can be shown over long times and demonstrates the stability of particle-stabilized bicontinuous gels. The particle interactions resist interface deformation and surface tension-driven coarsening, in particular. Both attractive and repulsive interactions can be used; see Ref. [19] for an appropriate parametrization of the SPFC model.

Finally, we demonstrate an important advantage of our multiscale model: The possibility of incorporating additional macroscopic effects using the diffuse domain approach [37]. We modeled a solid ball, driven by gravity, falling through a colloid crystallized surface. Compared to the case without colloids, the stiffness imparted to the interface by the colloids resisted the ball motion. At small to medium colloid elasticity the ball penetrated but did not fall through the interface as it would if the interface were clean. Interestingly, for higher elasticity the ball may not even penetrate the interface but reaches a steady position right above the interface. This clearly demonstrates the solid like properties of the particle-stabilized bicontinuous gel.

There are many interesting directions to pursue in the future. This includes developing methods to upscale the microscopic SPFC model and elastic force to obtain a fully macroscopic system, investigating the rheological properties of simulated bijels and comparing the results with physical systems (e.g., Refs. [38,39]), and developing a model of a cross-flow microreactor in which two fluids flow in opposite direction allowing close contact between mutually insoluble reagents across a colloid-stabilized interface in a bijel [6].

## ACKNOWLEDGMENTS

S.A. and A.V. acknowledge support from the German Science Foundation through grants Vo899/6, SFB 609 TP C10, and SPP-1506 Vo899/11. J.L. gratefully acknowledges partial support from the National Science Foundation Division of Mathematics and the National Institutes of Health through grant P50GM76516 for a Center of Excellence in Systems Biology at the University of California, Irvine. We acknowledge support of computing time at ZIH at TU Dresden and JSC at FZ Jülich.

[1] S. Pickering, J. Chem. Soc. **91**, 2001 (1907).
[2] A. B. Subramaniam, M. Abkarian, L. Mahadevan, and H. A. Stone, Nature (London) **438**, 930 (2005).
[3] C. Zeng, H. Bissig, and A. D. Dinsmore, Solid State Commun. **139**, 547 (2006).
[4] F. Leal-Calderon and V. Scmitt, Curr. Opin. Colloid Interface Sci. **13**, 217 (2008).
[5] E. Dickinson, Curr. Opin. Colloid Interface Sci. **15**, 40 (2010).
[6] K. Stratford, R. Adhikari, I. Pagonabarraga, J. C. Desplat, and M. E. Cates, Science **309**, 2198 (2005).

[7] E. M. Herzig, K. A. White, A. B. Schofield, W. C. Poon, and P. S. Clegg, Nat. Mater. **6**, 966 (2007).
[8] M. E. Cates and P. S. Clegg, Soft Matter **4**, 2132 (2008).
[9] A. J. C. Ladd, J. Fluid Mech. 271, (1994).
[10] A. J. C. Ladd, J. Fluid Mech. 271, (1994).
[11] A. J. C. Ladd and R. Verberg, J. Stat. Phys. **104**, 1191 (2001).
[12] A. S. Joshi and Y. Sun, Phys. Rev. E **79**, 066703 (2009).
[13] F. Jansen and J. Harting, Phys. Rev. E **83**, 046707 (2011).
[14] Paul C. Millett and Yu U. Wang, J. Colloid Interface Sci. **353**, 46 (2011).
[15] S. Aland, J. Lowengrub, and A. Voigt, Phys. Fluids **23**, 062103 (2011).
[16] K. R. Elder, M. Katakowski, M. Haataja, and M. Grant, Phys. Rev. Lett. **88**, 245701 (2002).
[17] K. R. Elder., N. Provatas, J. Berry, P. Stefanovic, and M. Grant, Phys. Rev. B **75**, 064107 (2007).
[18] S. van Teeffelen, R. Backofen, A. Voigt, and H. Löwen, Phys. Rev. E **79**, 051404 (2009).
[19] R. Backofen, M. Gräf, D. Potts, S. Praetorius, A. Voigt, and T. Witkowski, Multiscale Model. Sim. **9**, 314 (2011).
[20] K. E. Teigen, P. Song, J. Lowengrub, and A. Voigt, J. Comput. Phys. **230**, 375 (2010).
[21] J. H. J. Thijssen, A. B. Schofield, and P. S. Clegg, Soft Matter **7**, 7965 (2011).
[22] K.-A. Wu and P. W. Voorhees, Phys. Rev. B **80**, 125408 (2009).
[23] J. Lowengrub, A. Rätz, and A. Voigt, Phys. Rev. E **79**, 031926 (2009).
[24] Andreas Rätz and A. Voigt, Nonlinearity **20**, 177 (2007).
[25] A. Rätz and A. Voigt, Commun. Math. Sci. **4**, 575 (2006).
[26] K. E. Teigen, X. Li, J. Lowengrub, F. Wang, and A. Voigt, Commun. Math. Sci. **7**, 1009 (2009).
[27] Erich Hartmann, Comput.-Aided Geometric Design **16**, 355 (1999).
[28] S. Aland, A. Rätz, M. Röger, and A. Voigt, Multiscale Model. Simul. **10**, 82 (2012).
[29] S. Vey and A. Voigt, Comput. Visual. Sci. **10**, 57 (2007).
[30] T. A. Davis, ACM Trans. Math. Softw. **30**, 196 (2004).
[31] www.amdis-fem.org.
[32] S. Aland, J. S. Lowengrub, and A. Voigt, Comput. Model. Eng. Sci., 77 (2010).
[33] R. Backofen, A. Rätz, and A. Voigt, Philos. Mag. Lett. **87**, 813 (2007).
[34] R. Verfürth, *A Review of a Posteriori Error Estimation and Adaptive Mesh-Refinement Techniques*, Wiley-Teubner Series, Advances in Numerical Mathematics (Wiley-Teubner, Stuttgart, 1996), p. 127.
[35] J. S. Sohn, Y.-H. Tseng, Sh. Li, A. Voigt, and J. S. Lowengrub, J. Comput. Phys. **229**, 119 (2010).
[36] D. Jamet, D. Torres, and J. U. Brackbill, J. Comput. Phys. **182** 262 (2002).
[37] X. Li, J. S. Lowengrub, A. Rätz, and A. Voigt, Commun. Math. Sci. **7**, 81 (2009).
[38] P. Cicuta, E. J. Stancik, and G. G. Fuller, Phys. Rev. Lett. **90**, 236101 (2003).
[39] S. Reynaert, P. Moldenaers, and J. Vermant, Phys. Chem. Chem. Phys. **9**, 6463 (2007).